Geophysical Journal International

Geophys. J. Int. (2026) **247**, 1–23 https://doi.org/10.1093/gji/ggag316
Advance Access publication 2026 August 6
Research Paper

Single fault earthquake cycle complexity

Huiwen Sun [1,2] and Thorsten W. Becker [1,2,3]

[1] *Institute for Geophysics, Jackson School of Geosciences, The University of Texas at Austin, Austin, TX78758, USA. E-mail: sunh0021@utexas.edu*
[2] *Department of Earth and Planetary Sciences, Jackson School of Geosciences, The University of Texas at Austin, Austin, TX78712, USA*
[3] *Oden Institute for Computational Engineering and Sciences, The University of Texas at Austin, Austin, TX78712, USA*

Accepted 2026 August 4. Received 2026 August 3; in original form 2026 February 27

SUMMARY

Large earthquakes occur irregularly and often show limited resemblance to an ideal, periodic stick-slip cycle. Numerical models and laboratory experiments have reproduced transitions from periodic to quasi-periodic and irregular behaviour, yet the mechanisms controlling these transitions remain debated. Here, we analyse 3-D earthquake-cycle simulations governed by rate-and-state friction on a single dipping fault embedded in an elastic half-space. This provides a simple framework for isolating the roles of frictional dynamics, fault geometry and free-surface effects before analysing more complex setups. Our tests show that subtle numerical meshing choices beyond insufficient spatial resolution can influence cycle behaviour and, in some cases, lead to spuriously periodic solutions. In terms of the physical effects, we expect that the ratio between the seismogenic width, W, and the nucleation length, L_∞, $W' = W/L_\infty$ to be a primary control on earthquake-cycle behaviour. We further systematically vary fault dip, the down-dip transition between velocity-weakening and velocity-strengthening friction, and lateral velocity-strengthening bounds. Our results confirm that increasing W' promotes transitions from periodic to quasi-periodic and irregular earthquake cycles. However, we also find that fault dip and frictional heterogeneities can independently induce similar transitions and compete with the influence of W'. The effects of these perturbations are not fixed: the same change in fault dip or frictional properties may either stabilize or destabilize earthquake cycles depending on the cycle regime occupied by the reference model. Together, these findings highlight the sensitivity of physics-based earthquake-cycle simulations to both physical and numerical model assumptions. This has important implications for the interpretation of fault system dynamics and seismic hazard.

Key words: Seismic cycle; Numerical modelling; Dynamics and mechanics of faulting.

1 INTRODUCTION

Earthquakes arise from the seismically rapid release of mechanical energy accumulated in the brittle part of the lithosphere due to tectonic loading. For a perfectly homogeneous fault system—where earthquakes have the same size, geometry and stationary constitutive behaviour—one would expect regular stick-slip cycles to occur in order to release accumulated slip in regular sliding events (G.K. Gilbert 1884; W.F. Brace & J.D. Byerlee 1966). However, major earthquakes associated with breaking entire boundary segments are hardly ever close to periodic. One way to characterize such irregularity is by means of the coefficient of variation (CV), that is, the ratio of standard deviation to mean recurrence times (e.g. S.P. Nishenko & R. Buland 1987). For continental transforms, CV from paleoseismology is $\gtrsim 0.2$ (e.g. K.M. Scharer *et al.* 2011; J.D. Howarth *et al.* 2021). Therefore, although tectonic slip budgets must balance over sufficiently long timescales, earthquake recurrence exhibits enough variability to limit the predictive power of elastic-rebound-type models and their derivatives (e.g. Y.Y. Kagan *et al.* 2012).

It remains unclear whether earthquakes are inherently chaotic and fundamentally unpredictable, or whether they are in principle amenable to physics-based forecasting. This motivates work on the origin of earthquake complexity. As end-member reference models, time- and slip-predictable sequences of characteristic earthquakes predict event size from elapsed time since the previous rupture, or conversely, the time to the next event from the slip of the previous one (K. Shimazaki & T. Nakata 1980). Natural earthquake cycles, however, frequently deviate from these idealized patterns through rupture dynamics, transient loading, heterogeneous rock properties, fault system interactions and damage evolution. Determining whether earthquake complexity stems from intrinsic nonlinear physics within the system and/or from pre-existing heterogeneity (e.g. in material properties), and how those interact, is crucial for understanding fault dynamics.

Within this context, there is a rich history of exploring physics-based, numerical earthquake cycle models governed by friction laws on a simplified fault interface in a homogeneous elastic medium. A widely adopted constitutive framework for fault friction is rate-and-state friction (RSF), in which friction, f, depends on slip velocity, V, and an evolving state variable, θ (J.H. Dieterich 1979;

A.L. Ruina 1983). We can write this as

$$\frac{\tau}{\sigma} = f(v, \theta) = f_0 + a \ln\left(\frac{V}{V_0}\right) + \psi(\theta) \quad \text{where} \quad \psi = b \ln\left(\frac{V_0 \theta}{d_c}\right). \tag{1}$$

Here, τ and σ are the shear and (effective) normal stress, respectively, f_0 and V_0 are the reference friction and slip rate, respectively, and θ is here assumed to be governed by the 'aging' evolution law (J.H. Dieterich 1979):

$$\dot{\theta} = 1 - \frac{V\theta}{d_c}. \tag{2}$$

Parameters a and b determine the rate and state dependence of f and control stability, and the state variable θ can be viewed as the mean contact lifetime which evolves over a characteristic slip distance, d_c.

Early work showed that homogeneous, geometrically simple faults with RSF tend to generate relatively regular earthquake cycles (J.R. Rice 1993; B.E. Shaw & J.R. Rice 2000), provided the cohesive zone length $L_b = \frac{Gd_c}{b\sigma}$, where G is the shear modulus, is adequately resolved numerically (J.R. Rice 1993; A.M. Rubin & J.P. Ampuero 2005). However, even such simple fault models can exhibit a range of emergent behaviour and earthquake cycle models governed by laboratory-derived friction laws have captured a wide range of fault dynamics, including slow slip and partial ruptures (e.g. N. Lapusta & J.R. Rice 2003; Y. Liu & J.R. Rice 2007; A.M. Rubin 2008; N. Kato 2014; S. Barbot 2019; C. Cattania 2019; J. Gauriau *et al.* 2023). Similar complexity arising from simple fault geometries has also been explored in laboratory experiments (e.g. J.C. Gu *et al.* 1984; K. Im *et al.* 2020; S.B.L. Cebry *et al.* 2022). Moreover, higher order limit cycles and other signatures of low-dimensional deterministic chaos have been inferred in natural fault systems, such as for slow-slip events (D.R. Shelly 2010; A. Gualandi *et al.* 2020).

While self-organized, chaotic behaviour has long been suggested for earthquakes (e.g. P. Bak & C. Tang 1989), strict M.J. Feigenbaum (1978)-type period-doubling cascades and truly chaotic states have so far been demonstrated primarily in idealized systems. In a period-doubling cascade, the recurrence pattern doubles in period as a control parameter is varied, producing increasingly complex sequences of earthquake sizes before transitioning to chaos. These include coupled spring-slider models with inertia (J. Huang & D.L. Turcotte 1990), a single slider governed by a two-state-variable rate-and-state friction law (T.W. Becker 2000) and an isolated asperity model (N. Kato 2014), for example. In contrast, irregular sliding behaviour observed in laboratory settings might be better described by stochastic rather than nonlinear constitutive-law driven irregularity (A. Gualandi *et al.* 2023). While aspects of the behaviour of finite fault earthquake cycle models appear akin to chaotic states (e.g. N. Kato 2014; S. Barbot 2019; C. Cattania 2019; J. Gauriau *et al.* 2023), we here refer to such sequences mainly as 'irregular' since it has not necessarily been demonstrated that they satisfy all of the formal criteria of deterministic chaos, including the sensitive dependence on initial conditions as expressed by a positive Lyapunov exponent.

To understand the fundamental controls of earthquake cycle complexity, an additional length scale plays an important role. In general, the critical length for nucleation of rupture scales as (Y. Ida 1972):

$$L \propto \frac{G\Gamma}{\Delta\tau^2}, \tag{3}$$

where Γ is the effective fracture energy, and $\Delta\tau$ is the shear stress drop. For a given constitutive law, L can be related to kinematic properties, such as the minimum slip required for the development of instability when a spring-slider obeys rate-state friction (J.R. Rice & A.L. Ruina 1983). Considering the linear stability around a crack and RSF, one can derive a nucleation length L_∞ as (J.R. Rice 1993; A.M. Rubin & J.P. Ampuero 2005; Y. Liu & J.R. Rice 2007):

$$L_\infty \propto \frac{Gd_c}{\pi\sigma} \frac{b}{(b-a)^2}. \tag{4}$$

The difference $a - b$ is the logarithmic velocity derivative of the steady-state friction coefficient from eq. (1) with respect to slip velocity, and $k_c = \frac{\sigma(b-a)}{d_c}$ defines a critical elastic stiffness (J.R. Rice & A.L. Ruina 1983). The cycle dynamics on a fault with characteristic dimension, W, depends on the ratio

$$W' = \frac{W}{L_\infty}. \tag{5}$$

For example, Y. Liu & J.R. Rice (2007) showed that W' determines if faults exhibit slow, oscillatory motions or periodic and irregular events, and N. Kato (2014) demonstrated that partial ruptures and period-doubling occur on a single fault once the nucleation length exceeds a certain W'. By varying W', the earthquake cycle regime shifts from periodic to quasi-periodic and ultimately to possibly chaotic regimes (N. Kato 2014; Y. Wu & X. Chen 2014; S. Barbot 2019; C. Cattania 2019; J. Gauriau *et al.* 2023). While we know that for certain state evolution laws, L_∞ affects the rupture regime and b/a influences the timing of earthquake sequences (J.R. Rice & A.L. Ruina 1983; C. Cattania 2019), it remains unclear how broadly these findings generalize and to what extent mechanical interactions and fault geometry contribute to complexity.

We expect that in addition to W', fault dip and frictional heterogeneities also govern earthquake behaviours. For example, from a field perspective, abrupt along-strike variation in fault dip by $\sim 30^\circ$ has been proposed to be the key constraint on the spatial limit of partial ruptures along the Alpine Fault, New Zealand (J.D. Howarth *et al.* 2014; E. Warren-Smith *et al.* 2022). Along-strike segmentation and fault bends further influence the range of possible rupture scenarios (e.g. C.B. DuRoss *et al.* 2016) and modulate earthquake cycle behaviour in physics-based models (e.g. B. Duan & D.D. Oglesby 2005; S. Ozawa *et al.* 2023). Dip and down-dip curvature of slabs control seismic cycles at subduction zones primarily by constraining the width of the seismogenic zone (J. Biemiller *et al.* 2024). The effects of such geometrical complexity are meant to be captured in earthquake simulators which seek to explore the dynamics of entire fault networks (e.g. K. Richards-Dinger & J.H. Dieterich 2012; S.N. Ward 2012) and have been used to generate multicycle catalogues for the Alpine (J.D. Howarth *et al.* 2021) and the San Andreas systems (B.E. Shaw *et al.* 2025).

We are motivated to understand the relative contributions of fault interactions, tectonic loading and frictional heterogeneity to complex seismicity in such models, compared to the inherent dynamics of single faults, which appear, at times, underappreciated. To do so, we first need a more complete picture of how isolated faults can produce complex series of events. Aspects of such cycle complexity have been explored in several modelling and benchmarking studies (e.g. B.A. Erickson *et al.* 2020; J. Jiang *et al.* 2022), but we are not aware of a comprehensive discussion of the seismic cycle effects examined here, which we hope will help guide future analysis and modelling of more complex fault systems.

We perform a series of tests of quasi-dynamic rate-state friction earthquake cycle models, varying friction and fault dip for a planar fault in a homogeneous, elastic half-space. For all tests, we first restrict fault slip to be in the strike or dip direction for strike-slip and thrust faults, respectively, and assume normal stress to be time-independent and uniform to avoid fault (self) loading effects on recurrence times (e.g. T.W. Becker & H. Schmeling 1998; M. Bonafede & A. Neri 2000), for simplicity. While a depth-independent effective normal stress is a simplification, it can be rationalized by near-lithostatic pore fluid pressure gradients at seismogenic depths, which reduce the effective normal stress to values that vary only weakly with depth (e.g. J.R. Rice 1992).

We begin by comparing the nucleation patterns and recurrence intervals of earthquake cycles generated using subtly different meshing strategies. We assess the influence of numerical limitations associated with certain triangular dislocation formulations and examine how decreasing mesh resolution affects rupture behaviour. These tests identify a model configuration in which the results reflect physical processes rather than numerical artefacts. Turning to the physical controls on cycle complexity, we examine the effects of varying W' using two approaches, fixed W and fixed L_∞, testing both strike-slip and thrust fault cycles. Fault dip is varied to explore free-surface effects, and we test down-dip transition gradients between the velocity-strengthening and velocity-weakening regions of the fault. Lastly, we examine lateral frictional bounds and embed an along-strike frictional heterogeneity band of variable depth and extent. These efforts serve to illustrate a range of different controls on single fault cycle complexity.

2 NUMERICAL MODEL

A standard approach approximates earthquake cycles by the quasi-dynamic motion of frictional surfaces within a homogeneous medium (e.g. J.R. Rice 1993; N. Lapusta & J.R. Rice 2003; P. Segall & A.M. Bradley 2012; B.A. Erickson *et al.* 2020). We follow such implementation and use the numerical code of S. Ozawa *et al.* (2023), modelling a half-space governed by the static force balance, with stress tensor $\boldsymbol{\sigma} = \sigma_{ij}$,

$$\nabla \cdot \boldsymbol{\sigma} = 0, \tag{6}$$

and linear, isotropic elasticity as the constitutive law

$$\sigma_{ij} = K\epsilon_{kk}\delta_{ij} + 2G\left(\epsilon_{ij} - \frac{1}{3}\epsilon_{kk}\delta_{ij}\right), \quad i, j = 1, 2, 3, \tag{7}$$

where $\boldsymbol{\epsilon} = \epsilon_{ij}$ is the strain tensor,

$$\epsilon_{ij} = \frac{1}{2}\left(\frac{\partial u_i}{\partial x_j} + \frac{\partial u_j}{\partial x_i}\right), \tag{8}$$

K is the bulk modulus, and repeated indices imply summation. Here, $K = \frac{5}{3}G$, and $G = 32.04$ GPa. Stresses and velocities, $\boldsymbol{v} = \frac{\partial \boldsymbol{u}}{\partial t}$, are tracked on fault surfaces which obey RSF. Eqs (1)–(2) are regularized as (J.R. Rice *et al.* 2001):

$$\frac{\tau_i}{\sigma_i} = \mathrm{arcsinh}\left(\frac{V_i}{2V_0}\exp\left(\frac{\psi_i}{a}\right)\right), \tag{9}$$

with:

$$\frac{\mathrm{d}\psi_i}{\mathrm{d}t} = \frac{b}{d_c}\left[V_0 \exp\left(\frac{f_0 - \psi_i}{b}\right) - V_i\right]. \tag{10}$$

Stress changes at the centroid of each fault element due to slip on all other elements are computed using a boundary element method with Green's functions for constant-slip rectangular (Y. Okada 1992) or triangular (M. Nikkhoo & T.R. Walter 2015) planar dislocations. For a total of N cells in the input fault mesh, the shear stress changes on the ith element are represented as:

$$\Delta\tau_i = \sum_j^N A_{ij} D_j, \tag{11}$$

where D_j is the slip on the jth element and $A, B \in \mathbb{R}^{N\times N}$ are interaction matrices computed from the dislocation solutions. Combining the interaction matrix and the friction law, the shear stress changes are expressed as:

$$\frac{\mathrm{d}\tau_i}{\mathrm{d}t} = \sum_{j}^{N} A_{ij}V_j + \dot{\tau}_i - \frac{G}{2c_s}\frac{\mathrm{d}V_i}{\mathrm{d}t}, \tag{12}$$

where c_s is the shear wave speed, and $\dot{\tau}_i$ is the tectonic loading rates for shear stress on the ith element. The third term in eq. (12) is the radiation damping approximation of inertia (J.R. Rice 1993), hence 'quasi-dynamic'. The time evolution of the ODE system, comprising eqs (10) and a substituted form of (12) using the total derivative of V, is computed with a step size controlled fourth order Runge-Kutta scheme (S. Ozawa *et al.* 2023). The matrix vector multiplications required to evaluate the stressing rates are accelerated using hierarchical matrix approximations, as is standard practice, here using the HACApk library of A. Ida (2018) as implemented by S. Ozawa *et al.* (2023).

For our reference model, we use a fault plane that is 50 km long and 20 km wide and build a structured triangular mesh to provide insights for future models with complex geometries for which triangles are typically considered a suitable choice. The cell size Δx of each right-angled triangle is 80 m, which is the maximum cell size that satisfies model convergence tests (Section 3.1 and appendix). We adopt frictional parameters of $b = 0.02$, $a_{\min} = 0.01$ for the velocity-weakening zones and $a_{\max} = 0.03$ in the velocity-strengthening zones, $d_c = 0.02$ m, and $\sigma = 58$ MPa. This yields $L_b = 552$ m, satisfying the numerical stability criterion $L_b/\Delta x \gtrsim 3$ required for triangular and rectangular meshes (e.g. J.R. Rice 1993; A.M. Rubin & J.P. Ampuero 2005; S. Ozawa *et al.* 2023). The fault is loaded with backslip, where all mesh elements are prescribed a uniform plate convergence rate of $V_{\mathrm{pl}} = 10^{-9}\,\mathrm{m\,s^{-1}}$. With a vertical fault, events of equivalent moment magnitude $M \geq 6$ then occur approximately every 120 yr with an average shear stress drop of ~ 6 MPa, corresponding to 6 per cent of the initial shear stress level (Section 3.1).

We expect $a - b$ for crustal rocks to show temperature dependence, such that when combined with typical geothermal gradients, this leads to a transition from velocity-strengthening, stable behaviour ($a - b > 0$) near the surface, to velocity-weakening, unstable behaviour ($a - b < 0$) at intermediate depths, and back to stable creep at greater depths (S.T. Tse & J.R. Rice 1986; M. Blanpied *et al.* 1991). One can define depth-dependent profiles that approximate the frictional behaviour of plate boundaries, ranging from stable creep to unstable slip (e.g. Y. Liu & J.R. Rice 2009). Here we mainly focus on a simple distribution of frictional parameters inspired by benchmark cases for earthquake cycles (B.A. Erickson *et al.* 2020), which is meant to lead to regular, seismic (fast) ruptures for the reference case. The velocity-weakening region is 47 km long along strike and 17.5 km wide along dip, and is connected to the surrounding velocity-strengthening regions by a smooth transition.

As discussed by C. Cattania & P. Segall (2021), for example, quasi-dynamic models in an elastic medium have several limitations. First, the representation of rupture dynamics is only approximate: rupture propagation and termination are simplified because inertia and wave propagation are neglected (e.g. N. Lapusta *et al.* 2000; N. Lapusta & Y. Liu 2009; M.Y. Thomas *et al.* 2014). Secondly, the lack of off-fault inelasticity may lead to an overestimation of local stress perturbations (e.g. A.N. Poliakov *et al.* 2002; D. Andrews 2005). We therefore expect that relative comparisons between different fault setups within the quasi-dynamic approach are more meaningful than absolute comparisons with real fault dynamics.

3 RESULTS

3.1 Discretization and mesh sensitivity tests

Given the sensitivity of earthquake cycle computations to modelling choices, we investigated the effects of commonly employed boundary-element formulations and meshing approaches. Our geometries are simple, but we expect such modelling choices to compound when addressing more complete fault systems. In general, quadrilateral dislocations such as those of Y. Okada (1992) exhibit superior convergence properties compared to triangular elements (e.g. M. Nikkhoo & T.R. Walter 2015; M. Barall & T.E. Tullis 2016; S. Ozawa *et al.* 2023). Moreover, H. Noda (2025) showed that, if not paired and evaluated carefully, the Nikkhoo & Walter dislocations can produce inaccurate self-stress estimates which can lead to checkerboard patterns. Nevertheless, triangular dislocations remain widely used in earthquake-cycle modelling because they readily accommodate curved faults. We therefore evaluate how common meshing choices influence earthquake-cycle behaviour, even for planar fault models.

3.1.1 Mesh resolution

We first explore the effects of gradually decreasing structured mesh resolution for earthquake cycle results. We deliberately underresolve the nucleation dimension and test for any changes in cycle regimes and cumulative moment release (cf. J.R. Rice 1993). For a structured mesh, progressively coarsening the element size from our default of $\Delta x = 0.08$ to 0.3 km produces substantial changes in earthquake-cycle behaviour despite maintaining broadly similar cumulative moment release and average shear stress changes (Fig. 1). While nonlinear dynamics measures of complexity such as correlation dimension and Lyapunov exponents can provide insights (e.g. T.W. Becker 2000; S. Wang 2024), such methods can be impractical for limited time-series and require careful benchmarking.

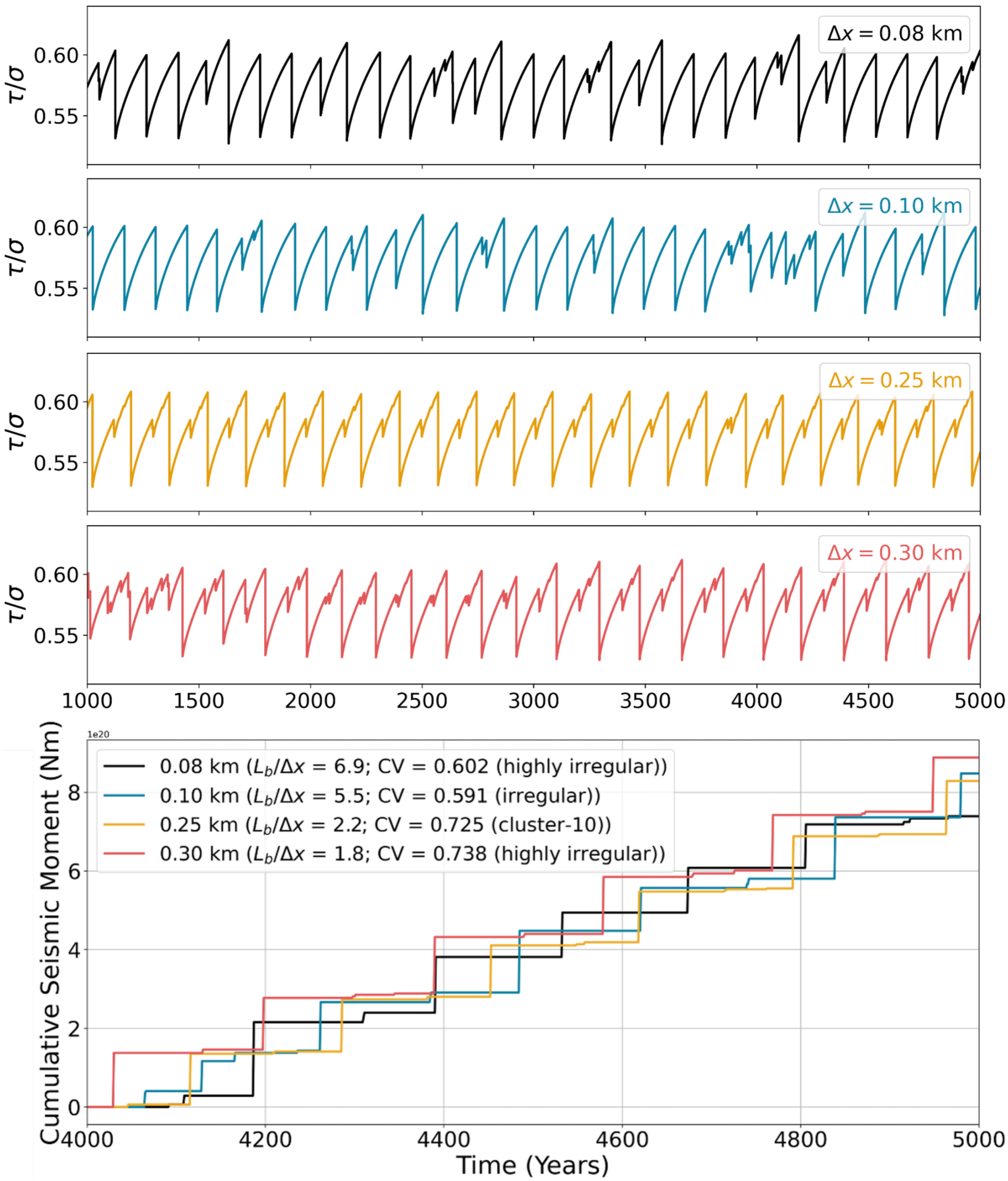

Figure 1. (top) Fault average friction coefficient time-series of models with gradually decreasing mesh resolution. (bottom) Cumulative moment release of models with different mesh resolutions, Δx. All cases share the same 10° dipping fault geometry with the same frictional setup.

We therefore use the simpler coefficient of variation (CV) of earthquake recurrence intervals to measure deviations from periodic recurrence throughout. The CV is defined as $\mathrm{CV} = \sigma_T/\bar{T}$, where $\bar{T}$ and σ_T are the mean and sample standard deviation of the inter-event times of events of all magnitudes, within the analysis window and excluding the initial spin-up phase. All cycles are categorized into four regularity levels: periodic ($\mathrm{CV} < 0.1$), semiperiodic ($0.1 \leq \mathrm{CV} < 0.3$), irregular ($0.3 \leq \mathrm{CV} < 0.6$) and highly irregular ($\mathrm{CV} \geq 0.6$). We note that higher period cycles, such as sequences repeating over several events, may exhibit elevated CV values, since CV measures the dispersion of recurrence intervals rather than their repeatability. We identify such cases to first order by counting the number N of characteristic recurrence times a sequence samples, treating intervals within 5 per cent of the median as the same value, and classify them as semiperiodic. We refer to these as cluster-N sequences, where N approximates the number of events per repeating sequence rather than implying true periodicity. At resolutions of 0.08 and 0.1 km ($L_b/\Delta x \approx 6.9$ and 5.5, respectively), both models generate irregular to highly irregular earthquake cycles characterized by predominantly system-wide ruptures ($7 \leq M \leq 7.5$), recurrence intervals of ~ 89 yr for events with $M \geq 6$, and comparable CV of 0.602 and 0.591. Although individual event sequences differ in detail, the overall recurrence statistics remain broadly consistent between the two resolutions.

Further coarsening the mesh to 0.25 and 0.3 km ($L_b/\Delta x \approx 2.2$ and 1.8) alters both the recurrence statistics and the rupture style (Fig. 1). The recurrence interval of events with $M \geq 6$ decreases to 54.5 and 49.1 yr, respectively. At 0.25 km resolution, the system exhibits an approximately cluster-10 sequence consisting of several partial ruptures followed by a system-wide event, indicating the emergence of an apparently regular rupture pattern absent in the finer resolution models. However, this behaviour does not persist at 0.3 km resolution, where recurrence intervals become more broadly distributed and the CV increases to 0.738. These results suggest that under-resolution can fundamentally alter the dynamical behaviour of the system, producing spurious periodicity in some cases and increased variability in others.

3.1.2 Mesh topology

In order to explore topological effects for the triangular mesh, structured meshes are generated by first dividing the fault plane into square cells and subsequently subdividing each cell into two triangular elements in either a regular or irregular fashion (Fig. 2). For the unstructured meshes, Delaunay-type meshing is used to generate both fully unstructured and quasi-structured meshes. While it is well known that finite element approaches can be affected by the artificial stiffness anisotropy introduced by regular meshing (e.g. R.H. MacNeal 1994) we do not expect boundary element models to suffer from such effects; nevertheless, an analogous sensitivity to element orientation might be expected from self-stress inaccuracies (H. Noda 2025).

At a mesh resolution of 0.1 km, earthquake cycles generated using the unstructured mesh deviate the most from those obtained using the structured and quasi-structured meshes (Fig. 2a). The recurrence interval is 61.9 yr for the unstructured mesh, compared to 63.4 and 63.5 yr for the structured and quasi-structured meshes, respectively. Refining the unstructured mesh to 0.09 km increases the recurrence interval to 63.1 yr. However, the 0.09 km unstructured mesh contains approximately 23 per cent more elements than the 0.1 km unstructured mesh and roughly 64 per cent more elements than the structured mesh, resulting in a substantially higher computational cost. Peak slip velocities are nearly identical between the two meshes, reaching $\sim$1.39 m s^{-1} in both cases, with the unstructured mesh higher by $\sim 10^{-4}$ m s^{-1}. A notable difference between the structured and unstructured meshes occurs in the interseismic locking pattern. In the unstructured mesh, a locked patch approximately 2 km wide persists near the centre of the fault immediately prior to rupture, whereas the locking zone is almost completely released in the structured mesh. This feature may be related to inaccuracies in stress evaluation between neighbouring triangular dislocations (H. Noda 2025). If so, the effect would be expected to be amplified in regions with strong velocity gradients near the rupture nucleation zone. The persistence of this locked patch is associated with slightly shorter recurrence intervals, possibly because a smaller locked area requires less stress accumulation before a fault-wide rupture occurs.

Increasing the mesh resolution reduces the size of the persistent locked patch. For the unstructured mesh, the width of the feature decreases from approximately 2 km at 0.1 km resolution to approximately 1 km at 0.09 km resolution. A similar feature is also observed when the diagonal connectivity of elements in the structured mesh is randomly flipped (Fig. 2b). While details of the implementation matter, recurrence intervals obtained using structured meshes with and without flipped connectivity converge to approximately 63.4 yr at a mesh resolution of 0.08 km. With these caveats in mind, in the models below, we use structured triangular meshing with a resolution of $\Delta x = 0.08$ km to ensure that the responses we analyse are robust within the range of our assumptions.

3.2 Physical effects on single fault cycle complexity

Fig. 3 provides an overview of the parameter space we explored using both strike-slip and thrust settings and summarizes our results in terms of fault dip, frictional and free surface effects on single fault cycle complexity. Consistent with previous studies, increasing W' generally promotes more complex earthquake-cycle behaviours, as indicated by the unstable region for both strike-slip and thrust faults. Semiperiodic to irregular sequences (CV ≥ 0.3) emerge for $W' \gtrsim 20$, whereas strongly irregular sequences (CV ≥ 0.6) are primarily observed for $W' \gtrsim 45$. However, W' alone does not fully determine cycle behaviour. Variations in fault dip, the gradient of the down-dip $a - b$ transition and the presence of lateral velocity-strengthening bounds can all modify the regularity of earthquake cycles. As shown in the insets of Fig. 3, greater irregularities (CV ≥ 0.3) are more commonly associated with more gradual down-dip $a - b$ transitions. However, the effects of changing fault dip and lateral frictional bounds are less systematic. In the following sections, we examine how these geometrical and frictional factors interact to produce transitions between periodic, semiperiodic and irregular earthquake sequences.

3.2.1 Effects of varying fault and nucleation dimensions

As shown by prior numerical work, smaller d_c leads to the appearance of partial ruptures (N. Lapusta *et al.* 2000), and fault and nucleation dimensions govern the transition from a periodic cycle regime to irregular regime of system-size and subsystem-size events (N. Kato 2014; Y. Wu & X. Chen 2014; S. Barbot 2019; C. Cattania 2019). We observe the same trend for both strike-slip and thrust faults on a dipping 2-D fault plane in an elastic half-space. Figs 4 and 5 show the transition from regular to irregular cycles on a strike-slip fault when W' is gradually increased. The exact value of W' at which the transition occurs differs across models of different frictional setups and dip angles. Irregular sequences appear at $W' \geq 50$ when W is fixed and L_∞ is varied, but occur at $W' \geq 22.7$ when L_∞ is

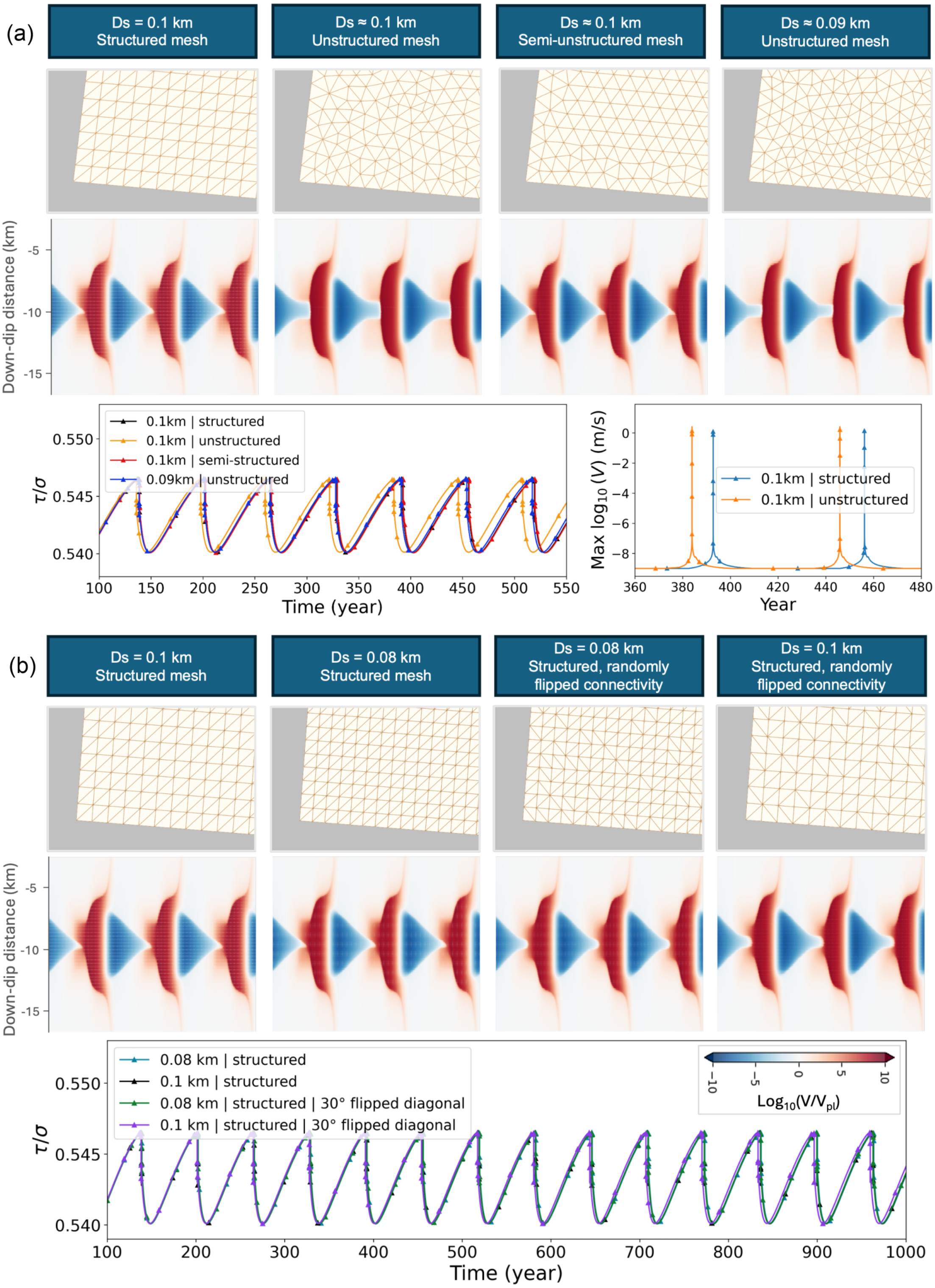

Figure 2. (a) Mesh structure, down-dip velocity time-series, fault average friction coefficient time-series and fault maximum slip velocity time-series of structured, unstructured and semi-unstructured triangular mesh models. (b) Mesh structure, down-dip velocity time-series and fault average friction coefficient time-series of structured triangular mesh models with and without flipped diagonals. The colourbar in (b) applies to all slip velocity panels in both (a) and (b).

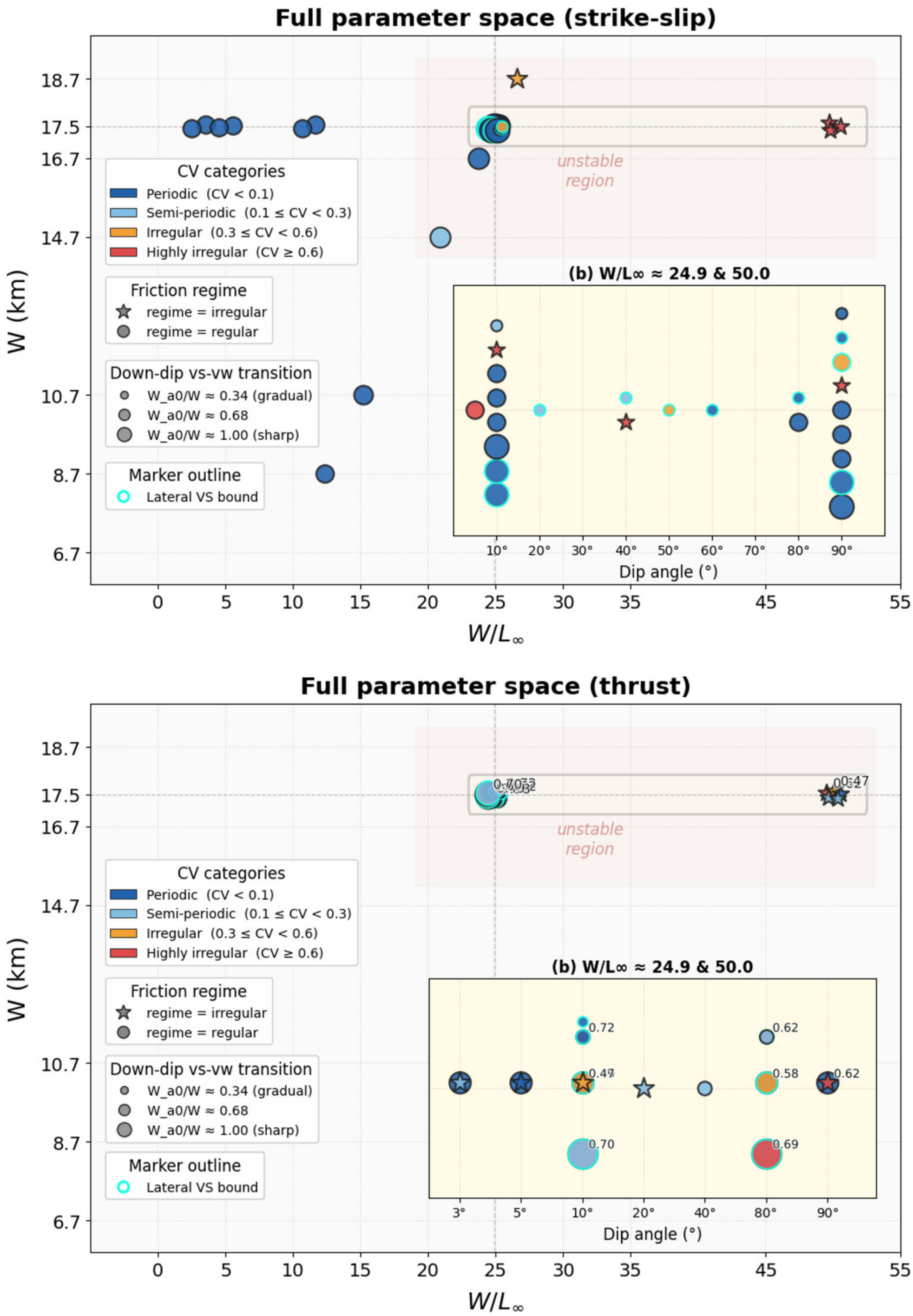

Figure 3. Parameter space explored for strike-slip (top) and thrust (bottom) faults. Each symbol corresponds to one earthquake cycle model run at a given parameter setup. For test cases varying the down-dip $a - b$ gradient while fixing both W and L_∞, larger symbol sizes indicate steeper gradients and vice versa. Cases with lateral frictional bounds are highlighted with symbol outlines, and cases with unstable frictional regime ($W' \geq 50$) have star symbols. For all cases, the coefficient of variation (CV) of the recurrence intervals of events of all magnitudes are classified by colour-coding. Inset shows the effect of dip angles and frictional heterogeneities on cycle regularity at a fixed W.

fixed and W is changed. There could also exist transient occurrences of semiregular cycles within the regular W' regime. For example, the earthquake cycle at $W' = 17.1$ has irregular recurrence intervals of system-size events, and a regular cycle at a slightly higher $W' = 19.9$ (Fig. 5). The W' values at which cycle periodicity changes may also depend on the aspect ratio of the fault plane, a factor that is not explored in this study. For all tests with a fixed W' in the following result sections, we refer to model setups with W' values that result in periodic to semiperiodic cycles as residing in a regular frictional regime and setups resulting in irregular cycles as having an irregular frictional regime.

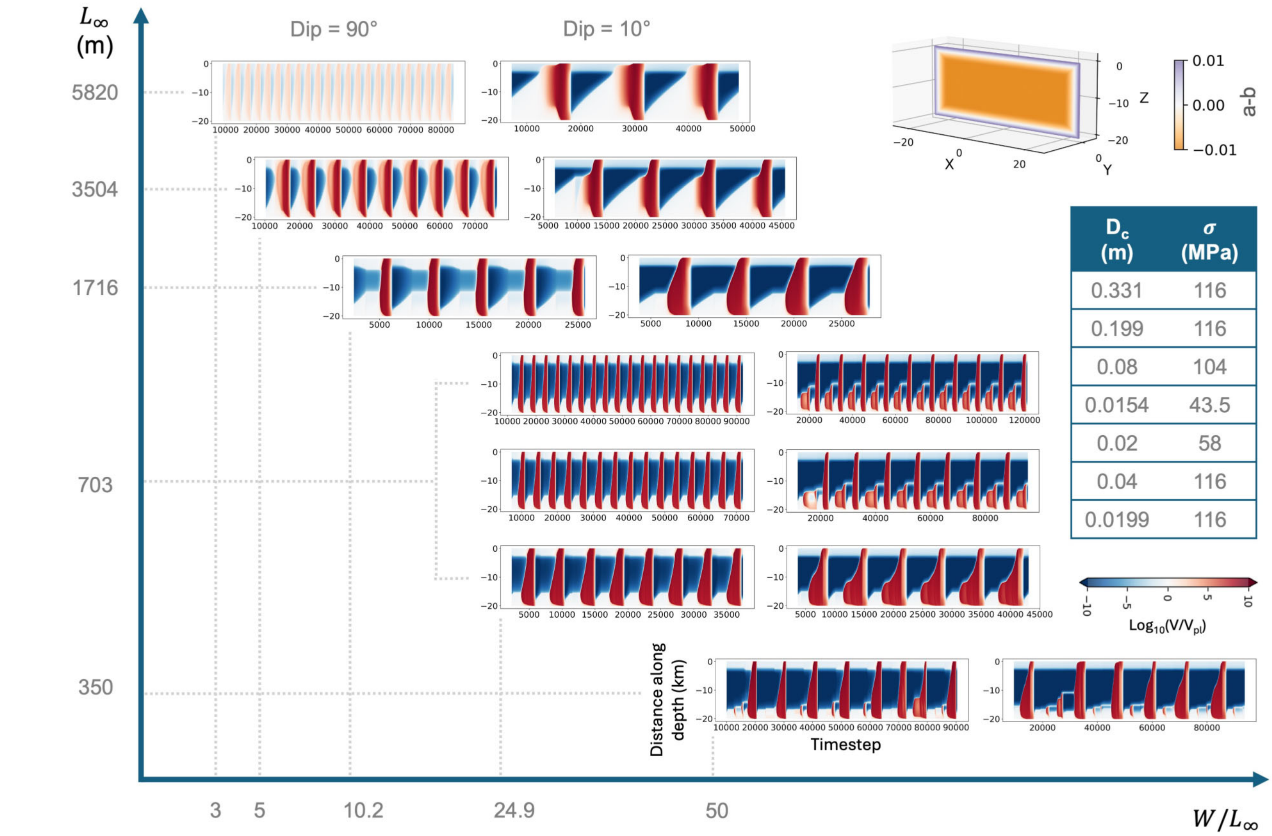

Figure 4. Effect of increasing L_∞ on cycle periodicity. Coloured panels show slip rate against time-step and down-dip distance along a vertical transect at the centre of the fault. The columns on the left and right are for a vertical and 10° dipping fault, respectively. All cases shown here are right-lateral strike-slip faults. The width of the velocity-weakening zone W is kept constant, while the nucleation length L_∞ is varied by changing the critical slip distance d_c and normal stress σ. Each row of the inset table corresponds to the model configuration shown in the same row of the slip-rate plots. Note that for the first two rows, the time frame shown is from year 600 to 5000, and for all other plots, the time range is from year 200 to 2000. The top right figure shows the frictional setup where the centre of the fault is velocity-weakening ($a - b < 0$), and the outermost circumference of the fault is velocity-strengthening ($a - b > 0$). The velocity-weakening and velocity-strengthening regions are linked by a transition zone with a gradual increase in $a - b$.

Reducing fault dip to 10° produces qualitatively different cycle behaviour depending on W'. At $W' = 3$, the vertical fault generates slow slip with maximum velocity $\sim 2.5 \times 10^{-7}$ m s^{-1} while the dipping fault produces coseismic slip with maximum velocity ~ 1 m s^{-1}. The occurrences of lower slip velocities at smaller W' have also been noted by Y. Liu & J.R. Rice (2007) and A.M. Rubin (2008). At $W' = 24.9$, the vertical fault produces periodic, full-fault events, whereas the dipping fault generates alternating partial and full-fault ruptures that resemble a period-doubling sequence. While the shallow dip of 10° is geometrically rare for continental transforms, the point here is not geometrical realism, but the shift in self-loading for tilted faults close to the surface, even when normal stress changes are neglected.

3.2.2 Effects of varying fault dips on cycle periodicity

The gradual transition from irregular to regular cycle sequence as the fault is tilted is shown in Fig. 6. We show recurrence time plots where inter event times are plotted against each other to detect period-doubling (Lorenz mappings) and phase-space plots (e.g. J.C. Gu *et al.* 1984; J.R. Rice & S.T. Tse 1986; T.W. Becker 2000), where dynamic time-series are condensed to mean velocity and stress on the fault. Given a starting model with irregular cycle regime at 10° dip, the system undergoes three transitional phases in terms of recurrence intervals as the dip angle increases in 10° increments (Fig. 6): At 20°, the earthquake cycle organizes into a repeating sequence of four event clusters on the recurrence plot, and each cluster corresponds to a characteristic sequence of short and long recurrence intervals. All clusters fall closer to the periodic recurrence line in the Lorenz mappings with a gradient of 0.5 and 2, reflecting alternating patterns of temporally closely spaced and widely separated events. Event clusters 1 and 4 are relatively compact, indicating more stable recurrence, whereas clusters 2 and 3 are more diffuse, showing greater variability from cycle to cycle. As the dip increases to 40°, the four event clusters merge into three, and at 60°, the cycle becomes fully periodic with only one repeating event at equal time intervals.

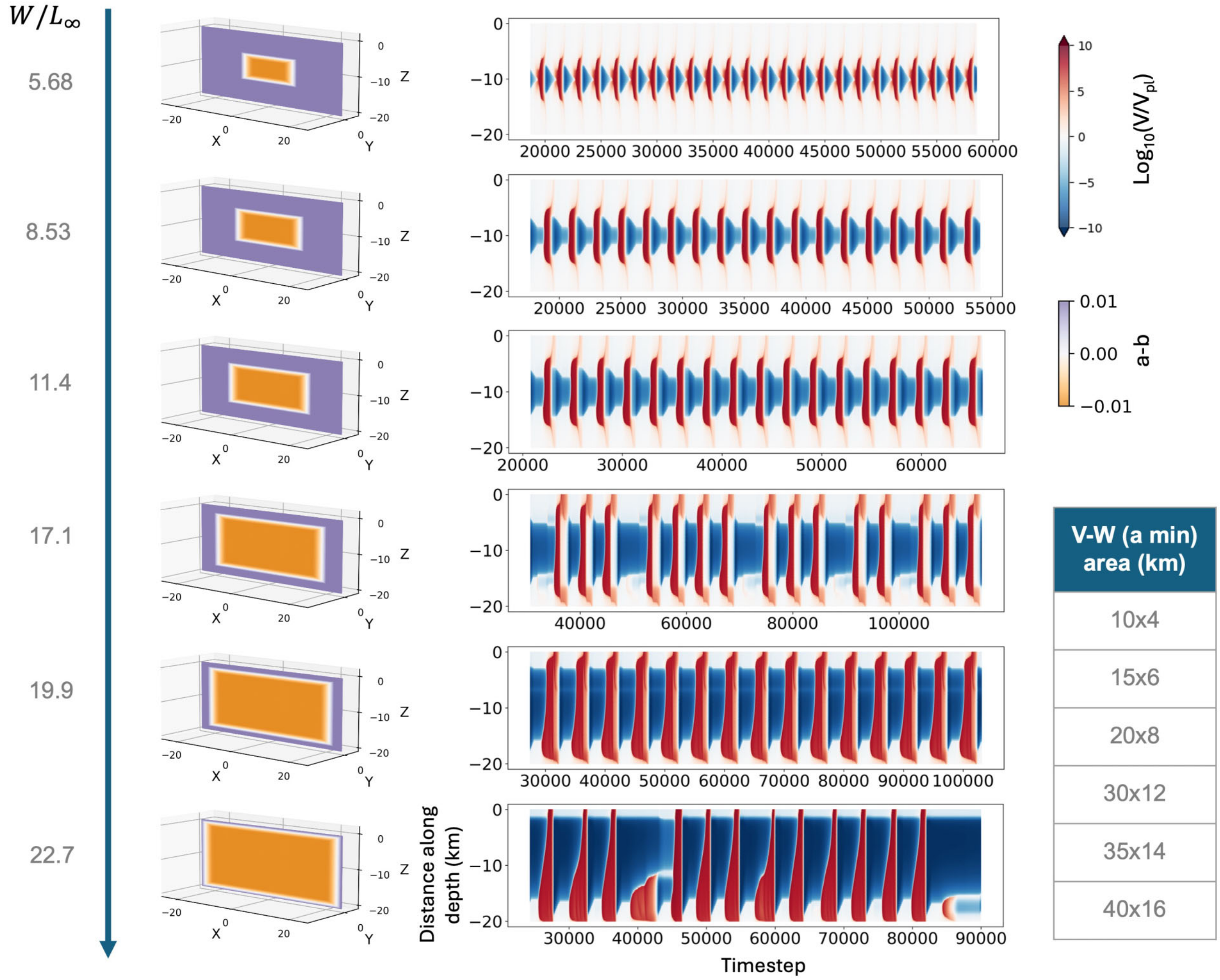

Figure 5. Effect of increasing W on cycle periodicity. Left column shows frictional setup and right shows the corresponding down-dip slip velocity time-series along a transect at the centre of the fault. All models show the results for a vertical strike-slip fault and share the same fault size and frictional parameter values. All slip rate plots show the time range of year 500 to 2000.

The complexity of the cycle regimes is also illustrated in the phase space trajectories of shear stress versus slip velocity (Fig. 6). The 10° dip case exhibits the most diverse trajectories, indicating a wide range of rupture behaviours. For dips between 20° and 40°, trajectories group into three to four distinct branches, corresponding to two smaller stress drops and one to two larger stress drops. At 60° and 80°, only one trajectory remains, consistent with a fully periodic cycle. Applying the same analysis to both strike-slip and thrust faults across frictional regimes (Fig. 7), we find that dip does not have a fixed-sign effect on cycle regularity; rather, its effect depends on the frictional regime of the fault. For faults with $W/L_\infty = 24.9$, which mostly generate irregular cycles at low dip, increasing dip promotes regularity for both strike-slip and thrust motion. For faults with $W/L_\infty = 50$, by contrast, increasing dip has little effect on the cycle periodicity of strike-slip faults, and even increases irregularity for thrust faults.

3.2.3 Interactions between fault dip and frictional heterogeneities

Motivated by the wide variability of frictional parameters observed experimentally, which can influence $a - b$ beyond the effects of temperature and lithology (e.g. D. Lockner *et al.* 1986; C. He *et al.* 2007; S.A. Den Hartog *et al.* 2014; R. Valdez *et al.* 2019), we investigate how the style of the down-dip $a - b$ transition influences earthquake-cycle periodicity. The depth range of the velocity-weakening zone is fixed ($z = -1.3$ to -18.8 km), while the transition into and out of the velocity-weakening region is varied from an abrupt step to a smooth symmetrical transition and an asymmetrical smooth transition (Fig. 8). In contrast to the reference models presented above, the models shown in Fig. 8 omit the lateral velocity-strengthening bounds, isolating the effect of the down-dip transition style; the bounds are reintroduced later in this section.

For shallowly dipping faults, earthquake cycle behaviour appears sensitive to the style of the frictional transition. For the 10° dipping strike-slip model, a sharp down-dip $a - b$ transition produces alternating partial and full-fault ruptures, resulting in a semiperiodic sequence with CV= 0.056. As the transition becomes more gradual, the system first evolves towards periodic full-fault ruptures

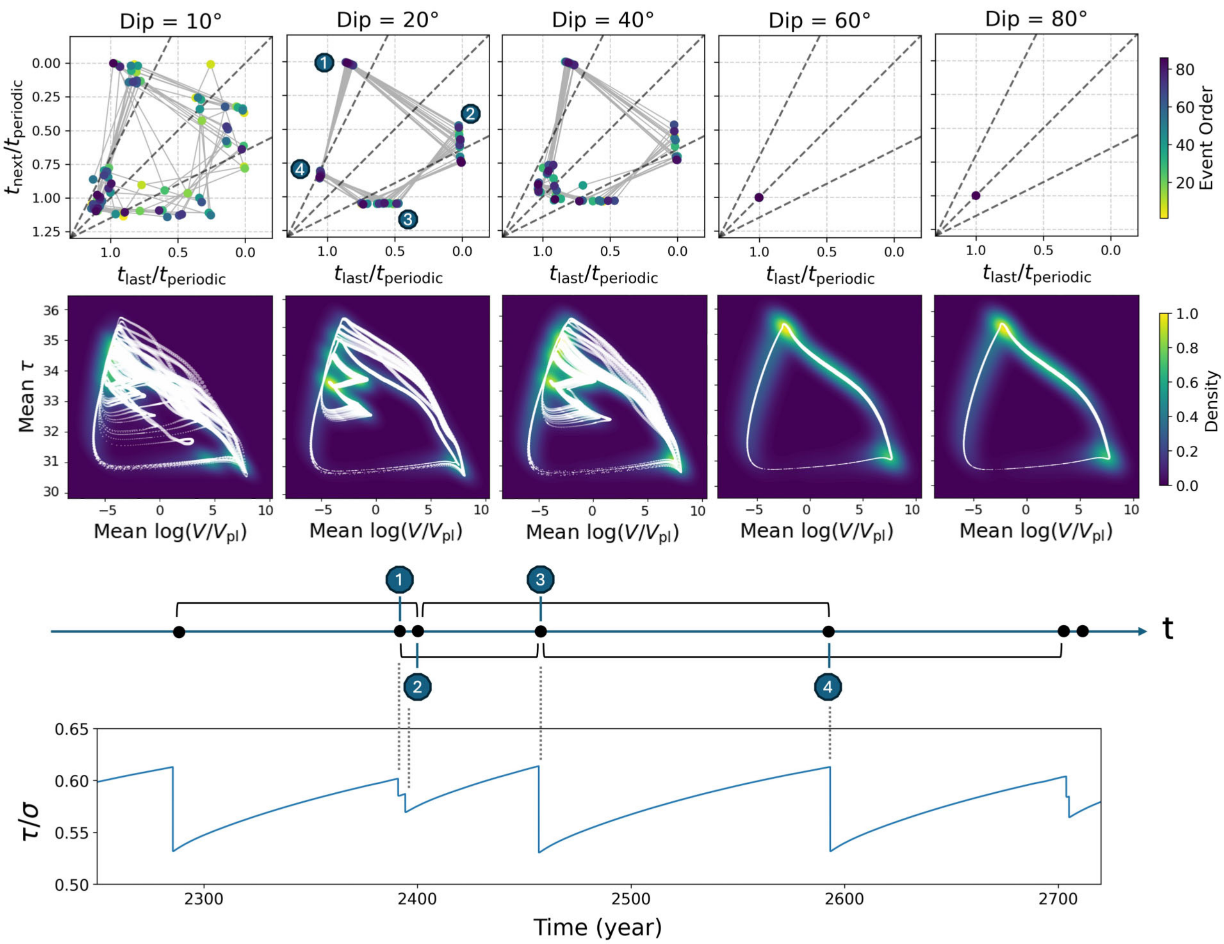

Figure 6. (top) Recurrence time plots (Lorenz mappings) where, for each earthquake in a cycle, the time to the next event is plotted against the time since the previous event. All recurrence times are normalized by the average recurrence time of the model with dip = 80°. Points are coloured by event order, and grey solid lines connect consecutive events. Each plot has three dotted linear lines with gradients 0.5, 1 and 2, indicating period-doubling and periodic cycles. (middle) Phase space plots showing cyclic changes in fault mean shear stress and slip velocity. Marker size is scaled with the standard deviations of stress and velocity. Background colourmap shows kernel density estimates (KDE) of stress on the fault plane through the cycle. Brighter spots corresponds to rupture initiations and terminations during which time-step sizes are smaller due to adaptive time stepping. (bottom) Friction time-series showing the repeating series of four event clusters for the model with 20° dip.

(CV= 0.0) and subsequently transitions to an irregular regime characterized by the coexistence of partial and full ruptures at non-repeating intervals (CV= 0.602). The symmetrical transition generates the largest and most regular earthquakes ($M \approx 7.3$, recurrence interval ≈ 148 yr), whereas the asymmetrical transition yields the broadest magnitude range ($M \approx 5.6$–7.4) and the shortest recurrence interval (≈ 86.8 yr). Since all models are loaded at the same backslip rate, larger earthquakes are generally associated with longer recurrence intervals, whereas smaller events recur more frequently to accommodate the same long-term slip budget. In contrast, vertical strike-slip faults remain periodic across all three transition profiles (Fig. 10), suggesting that sensitivity to the down-dip transition style is greatest at shallow dip.

To examine the combined effects of along-strike and down-dip frictional heterogeneity, we reintroduce the lateral velocity-strengthening bounds to faults with dip angles of 10° and 90° (Fig. 9a). For strike-slip faults with gradual (both symmetrical and asymmetrical) frictional transitions, removing the lateral bounds is associated with a shift from periodic to irregular cycles. For irregular cycles without lateral bounds, ruptures propagate outward in all directions and frequently terminate before spanning the entire fault plane (Fig. 9b). The resulting variability in rupture extent leaves behind a heterogeneous post-seismic stress field, which in turn modifies the conditions for subsequent nucleation and may sustain cycle-to-cycle irregularity. In contrast, models with lateral frictional bounds produce predominantly through-going ruptures and exhibit more regular recurrence patterns (Fig. 9b). For sharp down-dip frictional transitions, both models with and without lateral frictional bounds remain largely periodic, although rupture nucleation becomes less spatially consistent when the lateral bounds are removed. Earthquakes nucleate repeatedly at the lower left corner when lateral boundaries are present, whereas nucleation alternates between the corners and the centre of the lower fault edge when they are absent (Fig. 9c).

The lateral bounds also modulate the behaviour of thrust faults (Fig. 10), although their effect differs from that in the strike-slip models. For the 10° dipping thrust fault, sensitivity to the down-dip transition style emerges only when lateral bounds are present: the

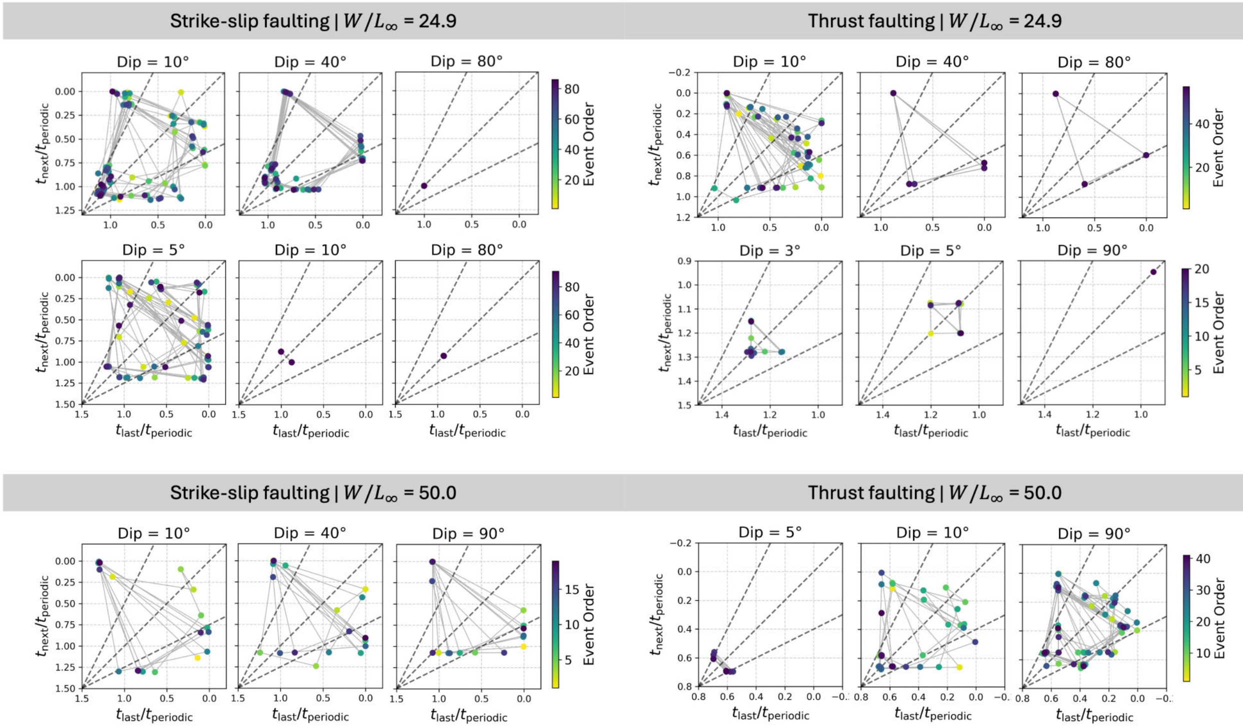

Figure 7. Recurrence time plots (Lorenz mappings). (top-left) Strike-slip faults in the regular dynamic regime with $W/L_\infty = 24.9$; (bottom-left) Strike-slip faults in the irregular regime with $W/L_\infty = 50$; (top-right) Thrust faults in the regular regime; (bottom-right) Thrust fault in the irregular regime with $W/L_\infty = 50$. Within the same panel, top and bottom rows show models with different down-dip $a - b$ transition gradients. Top row has a more gradual down-dip $a - b$ transition while bottom row has a sharper transition. For faults in the regular regime, increasing dip angle leads to more regular earthquake cycles while for fault in the irregular regime, the effect of increasing dip could either be less prominent or lead to greater irregularities.

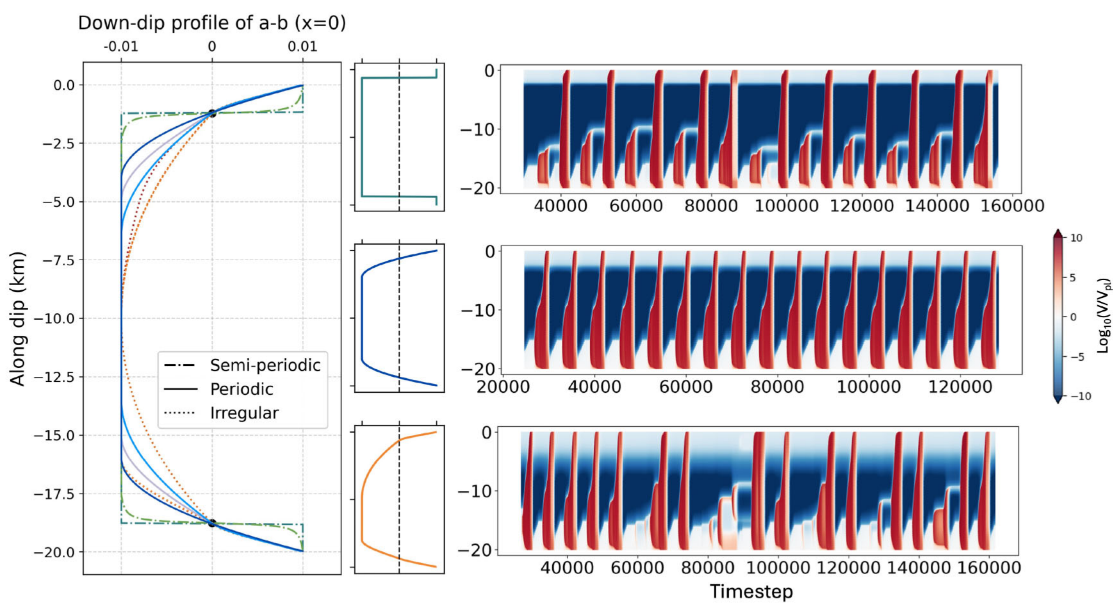

Figure 8. (left) Down-dip frictional profiles showing different transition gradients between the velocity-strengthening zone and the velocity-weakening zone. More abrupt changes in $a - b$ yield semiperiodic cycles (dash-dotted lines), intermediate transition gradients yield periodic cycles (solid lines), and more gradual transitions give irregular earthquake sequences (dotted lines). (right) All velocity time-series plots range from year 500 to 3000 on a 10° dipping strike-slip fault.

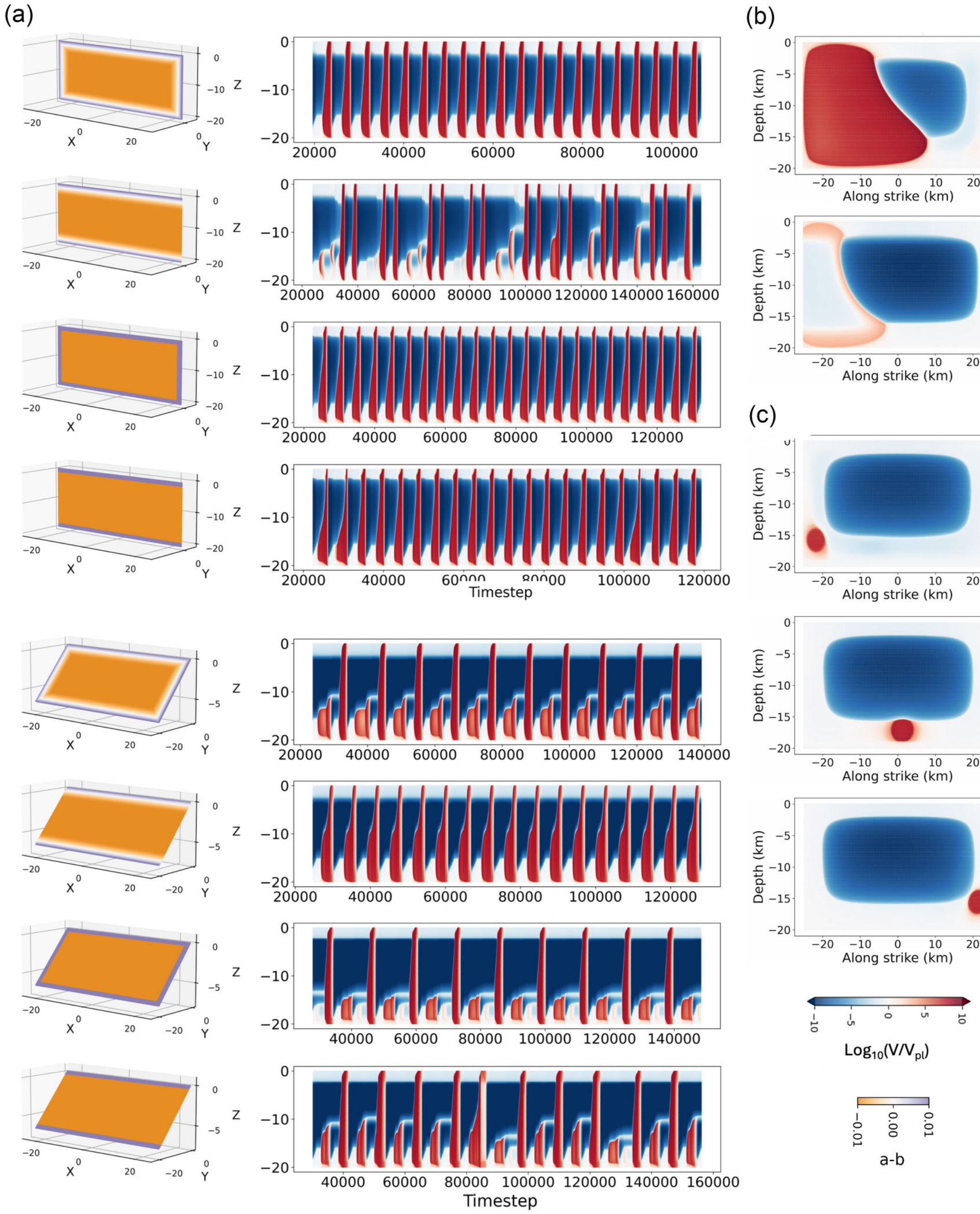

Figure 9. (a) Frictional setups with and without transition zones and/or lateral frictional boundaries on vertical and 10° dipping strike-slip faults. All velocity time-series range from year 500 to 3000. (b) Snapshots of slip velocity at selected time-steps from models in the first row of (a). (top) Through-going rupture when lateral frictional bounds are present. (bottom) Pre-mature rupture termination when lateral frictional bounds are absent. (c) Snapshots of slip velocity showing different rupture initiation points. (top) Repeating rupture initiation point at the lower left corner, corresponding to the model with lateral frictional bounds in the third row of (a). (middle and bottom) Changing rupture initiation points, corresponding to the model without lateral frictional bounds.

sharp transition and the asymmetrical gradual transition produce highly irregular cycles (CV= 0.702 and 0.723, respectively), while the symmetrical gradual transition yields a periodic cycle (CV= 0.003). Without lateral bounds, the cycles remain largely insensitive to the transition style. For the 80° dipping thrust fault—a geometry that is rare in nature owing to its inefficiency in accommodating tectonic strain—the transition style plays a minor role, and the addition of lateral bounds instead increases the periodicity of the modelled cycles. Across the models considered here, the influence of the lateral bounds is therefore comparable to, or stronger than, that of the down-dip $a - b$ transition gradient.

a-b down-dip transition	Strike-slip 10°		Strike-slip 90°		Thrust 10°		Thrust 80°		Average CV*
	No bound	With bound	No bound	With bound	No bound	With bound	No bound	With bound	
Sharp	Periodic 0.056	Periodic 0.016	Periodic 0.029	Periodic 0.000	Semi-periodic 0.262	Highly irregular 0.702	Highly irregular 0.691	Cluster-4* 0.648	0.301
Symmetrical gradual	Periodic 0.000	Periodic 0.068	Irregular 0.567	Periodic 0.001	Irregular 0.492	Periodic 0.003	Irregular 0.576	Periodic 0.000	0.213
Asymmetrical	Highly irregular 0.602	Cluster-3* 0.738	Periodic 0.000	Periodic 0.001	Periodic 0.045	Highly irregular 0.723	Highly irregular 0.616	Cluster-3* 0.779	0.438

Periodic (CV < 0.1)
Irregular (0.3 ≤ CV < 0.6)
Semi-periodic (0.1 ≤ CV < 0.3, or cluster-N*)
Highly irregular (CV ≥ 0.6)

Figure 10. Summary table showing cycle periodicity of three $a - b$ down-dip transition styles for strike-slip and thrust faults with shallowly dipping, near-vertical or vertical fault planes. The effects of the absence or presence of lateral velocity-strengthening frictional bounds are tested as well. Coefficient of variation (CV) of recurrence intervals as well as cycle regularity are labelled and colour-coded.

3.2.4 Frictional heterogeneity—barrier or perturbation?

Building on the tests of lateral and down-dip frictional controls, we now introduce additional along-strike frictional heterogeneity in the form of a localized velocity-strengthening band that extends across the fault width at a prescribed depth, with its down-dip width and position systematically varied. This is motivated by lithological and deformation-history controls on $a - b$ (e.g. D.M. Saffer & L.M. Wallace 2015) as well as the presence of strength heterogeneity and mixed rheological deformation regimes in exhumed plate boundaries (e.g. W.M. Behr & R. Bürgmann 2021). It is clear that heterogeneity in $a - b$ can lead to changes in event populations throughout the seismic cycle (e.g. R. Ito & Y. Kaneko 2023), but here we wish to focus on some basic tests as to how modulations, or 'noise', in material parameters affect simple cycles. We focus on two questions: whether a small perturbation to the $a - b$ profile can shift the cycle regime, and whether the outcome depends on the frictional regime the unperturbed model already occupies. All models in these tests omit the lateral velocity-strengthening bounds, so that the effects of the heterogeneous band are not conflated with those of the fault edges.

For a fixed width of the velocity-strengthening band, such frictional heterogeneity centred on the fault plane (within the velocity-weakening zone) perturbs the earthquake cycle most strongly (Fig. 11a), whereas bands placed entirely within the velocity-strengthening regions have a comparatively minor effect. This suggests that the seismogenic zone is more sensitive to small $a - b$ perturbations than the surrounding stable regions, consistent with the concentration of stress loading and nucleation within the velocity-weakening patch.

When the heterogeneity band is narrower ($\sim$ 200 m) than the nucleation length ($\sim$ 350 m), it does not systematically interfere with rupture initiation, propagation or rupture speed (Figs 11b and c). A thin velocity-weakening band located in the shallower velocity-strengthening region generates about three cycles of partial ruptures near $t = 1200$ yr ($\sim$8 times the reference recurrence interval) before the system returns to periodic behaviour. Here, imposed frictional complexity does lead to irregular-looking seismicity, but that seismicity heterogeneity is stationary in time and not truly 'complex' in that patterns eventually repeat themselves. When the heterogeneity band ($\sim$ 1000 m) exceeds the nucleation length, it acts as an effective barrier to rupture propagation (Fig. 11c), switching the cycle from regular to irregular. The barrier repeatedly arrests rupture, generating sequences of partial ruptures before a system-wide event breaks through. The earthquake cycle exhibits more complex behaviour, dominated by a repeating unit of three events—two with smaller stress drops followed by one large, system-wide rupture—interspersed with less regular events that show no particular periodicity. Around $t = 7000$ yr, a cluster of smaller but more frequent ruptures occurs intermittently. Adding a sinusoidal along-dip variation to the $a - b$ profile results in alternating down-dip zones of stronger and weaker interseismic locking, and produces a period-doubling regime.

To test whether these outcomes are controlled by the along-strike velocity-strengthening band or by the dynamical regime of the starting model, we apply the same set of bands to a second frictional profile at the same dip (Supplementary material Fig. S1) to compare with Fig. 11. For narrow bands, both starting profiles ultimately settle into periodic behaviour: the already-periodic model is only transiently perturbed, while the irregular model is pulled toward periodicity. For wider bands, the outcome diverges between profiles: the periodic starting model transitions to irregular behaviour as the barrier introduces variable rupture arrest, while the irregular starting model shifts to semiregular. The thick band therefore destabilizes a periodic system while incompletely regularizing an irregular one, rather than producing a clean sign-reversal. Together, these results show that neither band width alone nor starting regime alone determines the outcome; it is their interaction that governs how frictional heterogeneity modifies the earthquake cycle.

When dip is varied alongside the down-dip frictional profile, the picture becomes even more complex (Fig. 12). The response to the along-strike frictional bands shifts with dip in a regime-dependent manner: the instability introduced by reducing dip can, in

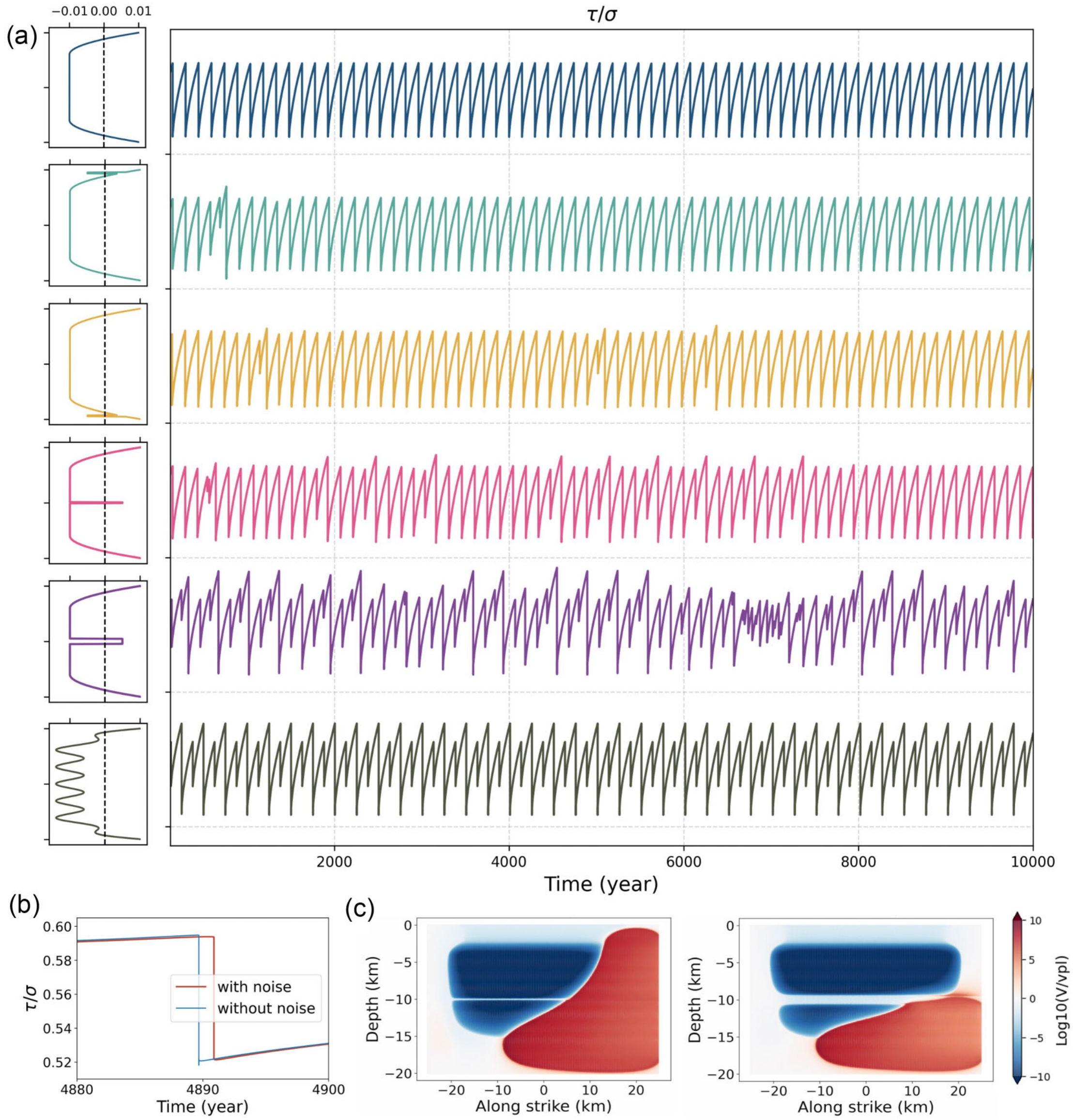

Figure 11. (a) Down-dip $a - b$ profiles and their corresponding friction coefficient time-series. All models have a 10° fault dip and no lateral frictional bounds. (b) Comparison of fault average friction coefficient of a full-system size rupture between models with and without frictional parameter perturbations. (c) Comparison of rupture propagation pattern between models with thin and thick velocity-strengthening bands.

some cases, be suppressed and replaced by more regular earthquake cycles when the frictional band is added. This stabilizing effect, however, is not universal. For the symmetrical frictional profile, the effect of dip is reversed, with cycles that are regular at 10° dip becoming increasingly irregular at steeper dips, and adding the along-strike frictional band does not suppress this irregularity but instead slightly enhances it. The influence of the frictional band therefore depends on the underlying dynamical state of the system, acting as a stabilizing or destabilizing perturbation depending on the regime.

4 DISCUSSION

4.1 Numerical issues when representing fault systems

4.1.1 Irregular seismicity from intrinsic nonlinearity versus numerical sensitivity

Similar to fault dip and frictional heterogeneities, the influence of mesh resolution on earthquake-cycle behaviour depends on the dynamical regime of the reference model. For models exhibiting regular cycles, decreasing the spatial resolution primarily alters recurrence intervals while preserving the overall rupture pattern (Fig. 2). In contrast, models that exhibit irregular behaviour at high resolution are substantially more sensitive to discretization. In these cases, progressively coarsening the mesh modifies both rupture

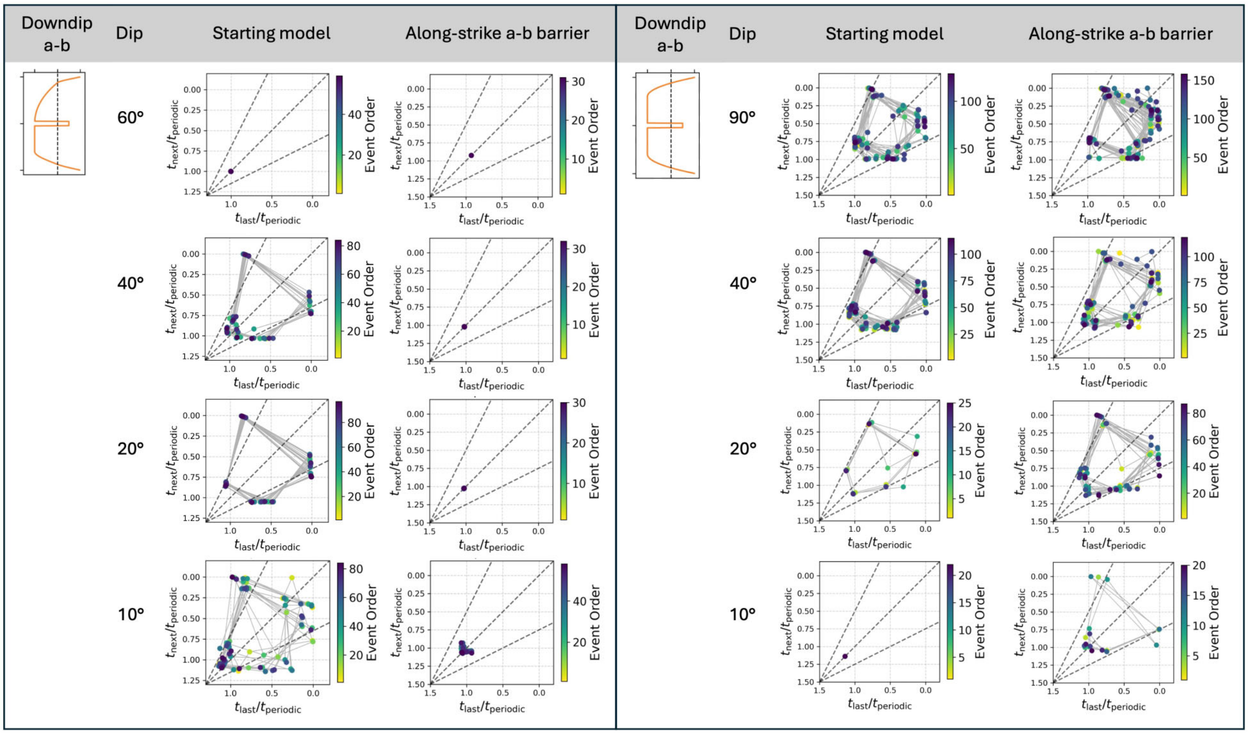

Figure 12. Recurrence time plots (Lorenz mappings) for test cases with varying down-dip $a - b$ gradients and dip angles, before and after an along-strike velocity-strengthening friction band is applied.

behaviour and earthquake-cycle regularity (Fig. 1). Our results are broadly consistent with the original findings of J.R. Rice (1993), who showed that insufficient spatial resolution can promote earthquake-cycle complexity. The relationship between resolution and complexity is not entirely monotonic, however. At 0.25 km, the model exhibits a higher order periodic sequence despite having a relatively lower resolution. While this behaviour may reflect a transient crossover into a neighbouring dynamical regime, the overall trend is toward increasing cycle complexity as the mesh becomes progressively under-resolved. This suggests that coarse discretization acts not simply as a source of numerical noise, but as a perturbation capable of modifying the underlying rupture dynamics.

Moreover, the emergence of numerical artefacts occurs even when L_b is nominally resolved by a few elements (Fig. 1). At resolutions of 0.25–0.30 km, the mesh is unable to adequately capture smaller scale stress and slip heterogeneities, resulting in earthquake sequences that differ substantially from those obtained using finer discretizations. This observation suggests that resolving nucleation dimensions alone may not be sufficient to recover the correct rupture regime necessarily.

4.1.2 Triangular meshing techniques

We examined which triangular meshing strategies yield robust earthquake-cycle behaviour and under what conditions (Section 3.1.2), and a number of approaches have been suggested to make the meshing itself more resilient to numerical artefacts. For example, M. Hyodo & T. Hori (2013) subdivided curved geometry faults into quadrilaterals, each of them was then approximated by three triangles. Our tests (not shown) confirm that this smoothing method can suppress self-stress checkerboards. H. Noda (2025) presented two approaches to mitigate numerical oscillations, with one focusing on subtracting the numerical artefact and the other using weighted multipoint evaluation to cancel the artefact, with focus on the forward computation of stresses. While we did not implement this fix in our models here, partially for the sake of argument, future work with triangular elements should implement M. Hyodo & T. Hori (2013) or H. Noda (2025) type corrections to reduce the effects of numerical inaccuracies.

Along with the need to super resolve L_b, these results highlight potentially underappreciated sources of variability among earthquake-cycle simulations and may contribute to observed discrepancies in benchmarks (B.A. Erickson *et al.* 2020; J. Jiang *et al.* 2022). Although differences in recurrence intervals are small (typically of order 1–3 per cent), they may nevertheless be relevant for studies focused on cycle predictability, rupture nucleation or model intercomparison. In addition, the details of nucleation and locking behaviour (e.g. Fig. 2) may be important when interpreting geodetic signals or other observations sensitive to near-nucleation fault processes.

4.2 The interplay between fault dip and frictional heterogeneities

4.2.1 Fault dip, segmentation, free-surface and the role of W'

For dipping faults, transitions from periodic to semiperiodic and eventually irregular earthquake cycles can arise through multiple mechanisms. Our results are broadly consistent with previous studies showing that increasing the ratio $W' = W/L_\infty$ promotes a progression from periodic to semiperiodic and ultimately irregular behaviour (e.g. N. Kato 2014; S. Barbot 2019; C. Cattania 2019), and that variations in frictional parameters within the rate-and-state framework can generate partial ruptures and a broad range of earthquake-cycle behaviours (e.g. N. Lapusta *et al.* 2000). C. Cattania (2019) showed that the fraction of system-size ruptures decreases systematically with W', eventually producing power-law distributed rupture sizes. S. Barbot (2019) showed that a scaled W' drives a bifurcation sequence from periodic slip through period-doubling to deterministic chaos, and found a similar progression for a single dipping thrust geometry. Our work substantiates these studies but highlights that the value of W' at which transitions occur shifts with fault dip. In addition, at constant W', changes in dip or frictional heterogeneity can either promote or suppress irregularity depending on the dynamical regime the system already occupies.

R.M. Skarbek (2025) showed that dip controls stability through the ratio of elastic stressing rate to frictional weakening rate, with shallower dips reducing the effective stiffness and promoting instability. This is consistent with our results near the regular frictional regime ($W' = 24.9$), where reducing dip shifts cycles toward greater irregularity. However, this relationship breaks down in the strongly irregular regime ($W' = 50$), where the same dip change does not consistently alter cycle regularity. The influence of the free surface may thus compete with, rather than universally dominate, the intrinsic frictional instability associated with large values of W'. This suggests that while the stressing-rate framework captures the onset of instability, the nonlinear dynamics far from the stability boundary are not fully described by linear stability analysis alone. We also note that R.M. Skarbek (2025) includes elastic normal stress perturbations generated by slip on dipping faults, whereas our models assume spatially and temporally uniform effective normal stress. Incorporating such normal stress feedbacks would likely shift the magnitude of the dip dependence and the locations of regime transitions, and would help clarify the relative contributions of geometric asymmetry and normal stress feedbacks to fault stability.

In more heterogeneous environments, additional sources of complexity may further obscure the influence of W'. For example, fractal variations in normal stress have been shown to modify earthquake-cycle regularity and may reduce the dominance of nucleation-length controls (e.g. J. Yun *et al.* 2025). Likewise, the critical nucleation length increases with the wavelength of frictional heterogeneity (P. Dublanchet 2018), suggesting that fault dimensions and frictional complexity are linked across spatial scales. Overall, our results indicate that fault dip influences not only the occurrence of instability, but also the style of the resulting earthquake cycle. Changes in dip modify the values of W' at which transitions between dynamical regimes occur, effectively expanding the parameter space governing earthquake-cycle behaviour. Within this broader parameter space, intermediate forms of complexity, including period-doubling and quasi-periodic sequences, emerge between regular and irregular regimes (e.g. T.W. Becker 2000; N. Kato 2014; S. Barbot 2019; A. Gualandi *et al.* 2023). The regime-dependent response to changes in dip further suggests that some model configurations may reside near transitions between dynamical states, such that relatively small geometric perturbations can produce substantial changes in earthquake-cycle behaviour.

4.2.2 Effects of frictional heterogeneity

In addition to W' and fault dip, frictional heterogeneities such as lateral frictional bounds and down-dip $a - b$ transitions can also govern cycle periodicity. First, irregular cycles emerge as the transition between velocity-weakening and velocity-strengthening regions becomes more gradual (Fig. 8). As discussed by S. Ray & R.C. Viesca (2017) and J. Jiang *et al.* (2022), such transition zones may host rupture nucleation when local stress conditions become more favourable than those in the velocity-weakening region. Wider transitional regions reduce the frictional contrast near the top of the seismogenic zone and could be more capable of hosting nucleation. In addition, more shallowly dipping faults are more sensitive to changes in the down-dip frictional profile, possibly because the free surface exerts a stronger influence on the along-dip stress field at low dip angles. From the perspective of geometric asymmetry, M. Aldam *et al.* (2016) showed that the loss of geometric reflection symmetry can fundamentally modify the stability of frictional sliding. Although their analysis addressed the linear stability of steady sliding rather than full earthquake-cycle dynamics, this broader principle provides conceptual support for our findings.

Lateral frictional bounds further modify cycle periodicity through two possible mechanisms. First, they reduce the effective along-strike width of the seismogenic region, altering the ratio of fault dimensions to the nucleation length and potentially shifting the system between dynamical regimes. Secondly, they impose barriers to rupture propagation, promoting more repeatable rupture extents and arrest locations. The latter effect may be particularly relevant to our models, where removing lateral bounds is associated with the emergence of partial ruptures and greater variability in rupture extent (Fig. 9). Such variability can produce more heterogeneous stress redistribution between events and may sustain cycle irregularity. Moreover, the contrasting effect of lateral frictional bounds on strike-slip versus thrust faults may arise from different effective W' which, along with the role of different free-surface normal stress interactions and the geometry of velocity-strengthening asperities, seems worthwhile to pursue.

The addition of along-strike frictional heterogeneity also changes cycle regimes, with a similar dependence on the regularity of the reference model (Figs 11 and S1, Supplementary material). Narrow bands smaller than the nucleation length act as net stabilizers regardless of the starting regime. Wide bands exceeding the nucleation length instead destabilize periodic systems by introducing variable rupture arrest, while regularizing irregular ones toward semiregular and regular behaviour. The outcome therefore depends jointly on band width and the dynamical state of the unperturbed system. Velocity-strengthening barriers are in general conditional (e.g Y. Kaneko *et al.* 2010), with rupture passage depending on barrier length, spacing and local stress conditions; a systematic exploration of these parameters remains a direction for future work.

When dip is additionally varied (Fig. 12), this regime dependence persists but interacts with free-surface effects and lateral frictional bounds in ways that are not straightforwardly additive. For the asymmetrical gradual down-dip $a - b$ transition, the destabilizing influence of reducing dip is offset by the introduction of an along-strike frictional band, shifting the system toward more regular earthquake cycles. However, this stabilizing effect is also not universal. For the symmetrical gradual transition, the effect of dip is reversed, with cycles that are regular at 10° dip becoming increasingly irregular at steeper dips. In this case, the along-strike frictional band does not alter the regularity regime, but slightly increases irregularity across the range of dip angles considered. One possible explanation is that the effectiveness of the along-strike frictional band depends on the degree of lateral confinement already present on the fault. In models where irregularity is primarily introduced by free-surface effects, the frictional band may promote more repeatable rupture segmentation by providing a persistent barrier to rupture propagation, thereby stabilizing the earthquake cycle. In contrast, when the absence of lateral velocity-strengthening boundaries is the dominant factor causing irregularity, ruptures can propagate freely along strike and exhibit substantial variability in rupture extent. Under these conditions, the along-strike band is unable to impose a consistent rupture pattern and instead interacts with an already heterogeneous stress field.

4.2.3 Regime-dependent responses to perturbations

Our results suggest that neither fault dip, down-dip frictional gradient, lateral velocity-strengthening boundaries, nor along-strike heterogeneity act as a monotonic control on earthquake-cycle regularity. Instead, the effect of each perturbation depends on the dynamical regime occupied by the system. Although we lack a unified theoretical description, the behaviour is broadly consistent with a bifurcation-boundary framework in which perturbations shift the system through a multidimensional parameter space. Under such a view, the same perturbation may stabilize one system while destabilizing another, depending on its proximity to a transition between dynamical regimes. A more complete understanding would require mapping the location of individual models relative to the relevant bifurcation boundaries, which is beyond the scope of this study. Transitions between periodic and irregular earthquake cycles can thus arise through multiple pathways, even in geometrically simple fault models with smooth frictional variations. Fault dip and frictional heterogeneity are closely coupled in controlling earthquake-cycle stability, and their effects may either reinforce or oppose one another depending on the underlying dynamical state of the system.

4.3 Real and numerical complexity

Earthquake-cycle complexity in numerical models can arise from either physical processes or numerical artefacts. This raises questions regarding the interpretation of earthquake simulator results used for seismic hazard assessment, as noted by V. Lambert & N. Lapusta (2021). Large-scale fault system models often require substantial simplifications and relatively coarse discretizations to represent complex fault networks. While such approximations may have limited influence on long-term moment release, they can significantly affect both quantitative measures, such as recurrence intervals, and qualitative characteristics of the resulting seismicity. Distinguishing genuine physical complexity from numerical artefacts therefore remains an important challenge for physics-based earthquake forecasting and probabilistic seismic hazard assessment.

From a nonlinear dynamics perspective, small shifts in frictional or geometric parameters can move the system across bifurcation thresholds, giving rise to apparently irregular or mixed-mode cycles even when the overall parameter regime is expected to produce regular behaviour. Models with control parameter choices near bifurcation boundaries can occupy narrow 'islands of stability' within an otherwise irregular parameter space. Such features are a hallmark of classical chaotic systems, such as Kolmogorov-Arnold-Moser (KAM) tori for three body problems. Bifurcation sequences along with islands of stability were shown to exist for the two-state variable rate-state friction spring-slider (T.W. Becker 2000) and, likewise, islands of chaos may exist for mainly periodic earthquake cycles for finite fault models (J. Gauriau *et al.* 2023). In cases with sensitive dependence not just on initial conditions but also on control parameter, both physical and numerical perturbations can shift the trajectory of the earthquake cycle towards a different parameter space regime.

4.4 Limitations of simplified models

Natural fault systems are characterized by additional processes, including spatially heterogeneous and time-dependent normal stress, viscoelastic relaxation in the surrounding medium, fluid pressure variations and dynamic stress transfer. These processes may introduce additional sources of complexity that either dominate or interact with the effects explored here. Nevertheless, our deliberately simplified framework demonstrates that isolated faults can already exhibit a broad spectrum of behaviours, ranging from periodic to quasi-periodic and irregular earthquake cycles. These behaviours arise solely from nonlinear interactions between geometric and frictional heterogeneity, providing a controlled framework for investigating how additional physical processes and fault-network interactions modify earthquake cycle dynamics. In particular, it would be valuable to investigate time-dependent normal stress and viscoelastic coupling to determine whether they generate fundamentally new behaviours or primarily modulate the dynamics already present in simpler systems.

5 CONCLUSIONS

We provide new insights into the controls of the complexity of the earthquake cycle for single faults and the mechanisms that drive transitions between periodic and irregular behaviour. We show that numerical implementation choices even for nominally well resolved models can influence cycle behaviour in subtle ways. Differences in meshing strategy and spatial resolution may generate artefacts that affect recurrence intervals, rupture nucleation and fault locking patterns, and in some cases can lead to spuriously regular solutions. This poses general challenges for complex fault system models.

In terms of the physical controls, we find that increasing the ratio of fault to frictional length scale, W', generally promotes more complex earthquake-cycle behaviour consistent with a range of previous work. However, we show that in addition to W', fault dip, down-dip frictional transitions, lateral frictional bounds and small-scale frictional heterogeneities can also substantially modify cycle regularity, even for isolated faults. The sensitivity to these perturbations can change sign: the same geometrical or frictional change may either stabilize or destabilize the earthquake cycle depending on the dynamical regime of the reference model. Our results further indicate that transitions between dynamical regimes may occur over a broader parameter space than previously recognized, with fault dip and frictional structure influencing not only the occurrence of instability but also the character of the resulting earthquake sequence.

The emergence of period-doubling, quasi-periodic and irregular behaviour in otherwise simple fault models underscores the rich nonlinear dynamics inherent to rate-and-state fault systems. Future work should focus on systematic exploration of bifurcation structures in parameter space, feedbacks with visco-elastic fault interactions and the identification of robust metrics for comparing modelled and observed earthquake sequences. Such efforts will be important for interpreting paleoseismicity and for assessing the reliability of physics-based fault system models in probabilistic seismic hazard analyses.

ACKNOWLEDGMENTS

We thank So Ozawa and colleagues for sharing their HBI software on https://github.com/sozawa94/hbi, Camilla Cattania and Andrew Bradley for comments on boundary elements, and Zhe Jia and two anonymous reviewers for their helpful comments on an earlier version of this paper. HS and TWB were partially supported by NSF EAR 2121666.

SUPPLEMENTARY MATERIAL

Supplementary materials are available at *GJIRAS* online.

suppl_data

Please note: Oxford University Press is not responsible for the content or functionality of any supplementary materials supplied by the authors. Any queries (other than missing material) should be directed to the corresponding author for the paper.

DATA AVAILABILITY

All simulations were performed with the open-source boundary element code HBI (S. Ozawa *et al.* 2023), available at https://github.com/sozawa94/hbi. The geometry files, frictional parameter files and event catalogues are archived on Zenodo at https://doi.org/10.5281/zenodo.21764218. A summary table mapping each model to the figure in which it appears, and listing its frictional parameters and recurrence statistics, is included in the archive.

REFERENCES

Aldam, M., Bar-Sinai, Y., Svetlizky, I., Brener, E.A., Fineberg, J. & Bouchbinder, E., 2016. Frictional sliding without geometrical reflection symmetry, *Phys. Rev. X,* **6,** 041023.
Andrews, D., 2005. Rupture dynamics with energy loss outside the slip zone, *J. geophys. Res.: Sol. Earth,* **110**.
Bak, P. & Tang, C., 1989. Earthquakes as a self-organized critical phenomenon, *J. geophys. Res.: Sol. Earth,* **94,** 15635–15637.
Barall, M. & Tullis, T.E., 2016. The performance of triangular fault elements in earthquake simulators, *Seismol. Res. Lett.,* **87,** 164–170.

Barbot, S., 2019. Slow-slip, slow earthquakes, period-two cycles, full and partial ruptures, and deterministic chaos in a single asperity fault, *Tectonophys.,* **768,** 228171.

Becker, T.W., 2000. Deterministic chaos in two state-variable friction sliders and the effect of elastic interactions, eds Rundle, J. B., Turcotte, D. L. & Klein, W., *GeoComplexity and the Physics of Earthquakes, vol. 120 of Geophys. Mono.,* American Geophysical Union, pp. 5–26.

Becker, T.W. & Schmeling, H., 1998. Earthquake recurrence-time variations with and without fault-zone interactions, *Geophys. J. Int.,* **135,** 165–176.

Behr, W.M. & Bürgmann, R., 2021. What's down there? The structures, materials and environment of deep-seated slow slip and tremor, *Phil. Trans. R. Soc. A,* **379**..

Biemiller, J., Gabriel, A.A., May, D. & Staisch, L., 2024. Subduction zone geometry modulates the megathrust earthquake cycle: magnitude, recurrence, and variability, *J. geophys. Res.: Sol. Earth,* **129,** e2024JB029191.

Blanpied, M., Lockner, D. & Byerlee, J., 1991. Fault stability inferred from granite sliding experiments at hydrothermal conditions, *Geophys. Res. Lett.,* **18,** 609–612.

Bonafede, M. & Neri, A., 2000. Effects induced by an earthquake on its fault plane: a boundary element study, *Geophys. J. Int.,* **141,** 43–56.

Brace, W.F. & Byerlee, J.D., 1966. Stick-slip as a mechanism for earthquakes, *Science,* **153,** 990–992.

Cattania, C., 2019. Complex earthquake sequences on simple faults, *Geophys. Res. Lett.,* **46,** 10384–10393.

Cattania, C. & Segall, P., 2021. Precursory slow slip and foreshocks on rough faults, *J. geophys. Res.: Sol. Earth,* **126,** e2020JB020430.

Cebry, S.B.L., Ke, C.Y., Shreedharan, S., Marone, C., Kammer, D.S. & McLaskey, G.C., 2022. Creep fronts and complexity in laboratory earthquake sequences illuminate delayed earthquake triggering, *Nature Commun.,* **13,** 6839.

Den Hartog, S.A., Saffer, D.M. & Spiers, C.J., 2014. The roles of quartz and water in controlling unstable slip in phyllosilicate-rich megathrust fault gouges, *Earth Planet. Space,* **66,** 1–9.

Dieterich, J.H., 1979. Modeling of rock friction: 1. Experimental results and constitutive equations, *J. geophys. Res.: Sol. Earth,* **84,** 2161–2168.

Duan, B. & Oglesby, D.D., 2005. Multicycle dynamics of nonplanar strike-slip faults, *J. geophys. Res.: Sol. Earth,* **110**..

Dublanchet, P., 2018. The dynamics of earthquake precursors controlled by effective friction, *Geophys. J. Int.,* **212,** 853–871.

DuRoss, C.B., Personius, S.F., Crone, A.J., Olig, S.S., Hylland, M.D., Lund, W.R. & Schwartz, D.P., 2016. Fault segmentation: New concepts from the Wasatch fault zone, Utah, USA, *J. geophys. Res.: Sol. Earth,* **121,** 1131–1157.

Erickson, B.A. *et al.*, 2020. The community code verification exercise for simulating sequences of earthquakes and aseismic slip (seas), *Seismol. Res. Lett.,* **91,** 874–890.

Feigenbaum, M.J., 1978. Quantitative universality for a class of nonlinear transformations, *J. Stat. Phys.,* **19,** 25.

Gauriau, J., Barbot, S. & Dolan, J.F., 2023. Islands of chaos in a sea of periodic earthquakes, *Earth planet. Sci. Lett.,* **618,** 118274.

Gilbert, G.K., 1884. A theory of the earthquakes of the Great Basin, with a practical application, *Am. J. Sci. Ser.,* **3,** 49–54.

Gu, J.C., Rice, J.R., Ruina, A.L. & Tse, S.T., 1984. Slip motion and stability of a single degree of freedom elastic system with rate and state dependent friction, *J. Mech. Phys. Solids,* **32,** 167–196.

Gualandi, A., Avouac, J.P., Michel, S. & Faranda, D., 2020. The predictable chaos of slow earthquakes, *Sci. Adv.,* **6,** eaaz5548.

Gualandi, A., Faranda, D., Marone, C., Cocco, M. & Mengaldo, G., 2023. Deterministic and stochastic chaos characterize laboratory earthquakes, *Earth planet. Sci. Lett.,* **604,** 117995.

He, C., Wang, Z. & Yao, W., 2007. Frictional sliding of gabbro gouge under hydrothermal conditions, *Tectonophysics,* **445,** 353–362.

Howarth, J.D., Fitzsimons, S.J., Norris, R.J. & Jacobsen, G.E., 2014. Lake sediments record high intensity shaking that provides insight into the location and rupture length of large earthquakes on the Alpine Fault, New Zealand, *Earth Planet. Sci. Lett.,* **403,** 340–351.

Howarth, J.D. *et al.*, 2021. Spatiotemporal clustering of great earthquakes on a transform fault controlled by geometry, *Nature Geosci.,* **14,** 314–320.

Huang, J. & Turcotte, D.L., 1990. Are earthquakes an example of deterministic chaos?, *Geophys. Res. Lett.,* **17,** 223–226.

Hyodo, M. & Hori, T., 2013. Re-examination of possible great interplate earthquake scenarios in the Nankai Trough, southwest Japan, based on recent findings and numerical simulations, *Tectonophys.,* **600,** 175–186.

Ida, A., 2018. Lattice H-matrices on distributed-memory systems. *2018 IEEE International Parallel and Distributed Processing Symposium (IPDPS),* pp. 389–398.

Ida, Y., 1972. Cohesive force across the tip of a longitudinal-shear crack and Griffith's specific surface energy, *J. geophys. Res.: Sol. Earth,* **77,** 3796–3805.

Im, K., Saffer, D., Marone, C. & Avouac, J.P., 2020. Slip-rate-dependent friction as a universal mechanism for slow slip events, *Nature Geosci.,* **13,** 705–710.

Ito, R. & Kaneko, Y., 2023. Physical mechanism for a temporal decrease of the Gutenberg-Richter *b*-value prior to a large earthquake, *J. geophys. Res.: Sol. Earth,* **128,** e2023JB027413.

Jiang, J. *et al.*, 2022. Community-driven code comparisons for three-dimensional dynamic modeling of sequences of earthquakes and aseismic slip, *J. geophys. Res.: Sol. Earth,* **127,** e2021JB023519.

Kagan, Y.Y., Jackson, D.D. & Geller, R.J., 2012. Characteristic earthquake model, 1884–2011, R.I.P, *Seismol. Res. Lett.,* **83,** 951–953.

Kaneko, Y., Avouac, J.P. & Lapusta, N., 2010. Towards inferring earthquake patterns from geodetic observations of interseismic coupling, *Nature Geosc.,* **3,** 363–369.

Kato, N., 2014. Deterministic chaos in a simulated sequence of slip events on a single isolated asperity, *Geophys. J. Int.,* **198,** 727–736.

Lambert, V. & Lapusta, N., 2021. Resolving simulated sequences of earthquakes and fault interactions: Implications for physics-based seismic hazard assessment, *J. geophys. Res.: Sol. Earth,* **126,** e2021JB022193.

Lapusta, N. & Liu, Y., 2009. Three-dimensional boundary integral modeling of spontaneous earthquake sequences and aseismic slip, *J. geophys. Res.: Sol. Earth,* **114**..

Lapusta, N. & Rice, J.R., 2003. Nucleation and early seismic propagation of small and large events in a crustal earthquake model, *J. geophys. Res.: Sol. Earth,* **108**..

Lapusta, N., Rice, J.R., Ben-Zion, Y. & Zheng, G., 2000. Elastodynamic analysis for slow tectonic loading with spontaneous rupture episodes on faults with rate-and state-dependent friction, *J. geophys. Res.: Sol. Earth,* **105,** 23765–23789.

Liu, Y. & Rice, J.R., 2007. Spontaneous and triggered aseismic deformation transients in a subduction fault model, *J. geophys. Res.: Sol. Earth,* **112**..

Liu, Y. & Rice, J.R., 2009. Slow slip predictions based on granite and gabbro friction data compared to GPS measurements in northern Cascadia, *J. geophys. Res.: Sol. Earth,* **114**..

Lockner, D., Summers, R. & Byerlee, J., 1986. Effects of temperature and sliding rate on frictional strength of granite, *Pure appl. Geophys.,* **124,** 445–469.

MacNeal, R.H., 1994. *Finite elements: Their Design and Performance,* Marcel Dekker.

Nikkhoo, M. & Walter, T.R., 2015. Triangular dislocation: an analytical, artefact-free solution, *Geophys. J. Int.,* **201,** 1119–1141.

Nishenko, S.P. & Buland, R., 1987. A generic recurrence interval distribution for earthquake forecasting, *Bull. seism. Soc. Am.,* **77,** 1382–1399.

Noda, H., 2025. Inconsistency of a single-point evaluation of traction on a fault discretized with triangular elements and several improved methods, *Earth Planet. Space,* **77,** 128.
Okada, Y., 1992. Internal deformation due to shear and tensile faults in a half-space, *Bull. seism. Soc. Am.,* **82,** 1018–1040.
Ozawa, S., Ida, A., Hoshino, T. & Ando, R., 2023. Large-scale earthquake sequence simulations on 3-d non-planar faults using the boundary element method accelerated by lattice h-matrices (version 2025.10.0) [software], *Geophys. J. Int.,* **232,** 1471–1481.
Poliakov, A.N., Dmowska, R. & Rice, J.R., 2002. Dynamic shear rupture interactions with fault bends and off-axis secondary faulting, *J. geophys. Res.: Sol. Earth,* **107,** ESE–6.
Ray, S. & Viesca, R.C., 2017. Earthquake nucleation on faults with heterogeneous frictional properties, normal stress, *J. geophys. Res.: Sol. Earth,* **122,** 8214–8240.
Rice, J.R., 1992. Fault stress states, pore pressure distributions, and the weakness of the San Andreas fault, eds Evans, B. & Wong, T.-F., *Fault Mechanics and Transport Properties of Rocks, vol. 51,* Academic Press, pp. 475–503.
Rice, J.R., 1993. Spatio-temporal complexity of slip on a fault, *J. geophys. Res.: Sol. Earth,* **98,** 9885–9907.
Rice, J.R. & Ruina, A.L., 1983. Stability of steady frictional slipping, *J. Appl. Mech.,* **50,** 343–349.
Rice, J.R. & Tse, S.T., 1986. Dynamic motion of a single degree of freedom system following a rate and state dependent friction law, *J. geophys. Res.: Sol. Earth,* **91,** 521–530.
Rice, J.R., Lapusta, N. & Ranjith, K., 2001. Rate and state dependent friction and the stability of sliding between elastically deformable solids, *J. Mech. Phys. Solids,* **49,** 1865–1898.
Richards-Dinger, K. & Dieterich, J.H., 2012. RSQSim earthquake simulator, *Seismol. Res. Lett.,* **83,** 983–990.
Rubin, A.M., 2008. Episodic slow slip events and rate-and-state friction, *J. geophys. Res.: Sol. Earth,* **113**.
Rubin, A.M. & Ampuero, J.P., 2005. Earthquake nucleation on (aging) rate and state faults, *J. geophys. Res.: Sol. Earth,* **110**..
Ruina, A.L., 1983. Slip instability and state variable friction laws, *J. geophys. Res.: Sol. Earth,* **88,** 10359–10370.
Saffer, D.M. & Wallace, L.M., 2015. The frictional, hydrologic, metamorphic and thermal habitat of shallow slow earthquakes, *Nature Geosc.,* **8,** 594–600.
Scharer, K.M., Biasi, G.P. & Weldon, R.J., 2011. A reevaluation of the Pallett Creek earthquake chronology based on new AMS radiocarbon dates, San Andreas fault, California, *J. geophys. Res.: Sol. Earth,* **116**.
Segall, P. & Bradley, A.M., 2012. Slow-slip evolves into megathrust earthquakes in 2D numerical simulations, *Geophys. Res. Lett.,* **39**..
Shaw, B.E. & Rice, J.R., 2000. Existence of continuum complexity in the elastodynamics of repeated fault ruptures, *J. geophys. Res.: Sol. Earth,* **105,** 23791–23810.
Shaw, B.E., Milner, K.R. & Goulet, C.A., 2025. Deterministic physics-based earthquake sequence simulators match empirical ground-motion models and enable extrapolation to data-poor regimes: Application to multifault multimechanism ruptures, *Seismol. Res. Lett.,* **96,** 2431–2444.
Shelly, D.R., 2010. Periodic, chaotic, and doubled earthquake recurrence intervals on the deep San Andreas Fault, *Science,* **328,** 1385–1388.
Shimazaki, K. & Nakata, T., 1980. Time-predictable recurrence model for large earthquakes, *Geophys. Res. Lett.,* **7,** 279–282.
Skarbek, R.M., 2025. The stability of frictional sliding on dip-slip and finite length faults, *Geophys. J. Int.,* **241,** 826–839.
Thomas, M.Y., Lapusta, N., Noda, H. & Avouac, J.P., 2014. Quasi-dynamic versus fully dynamic simulations of earthquakes and aseismic slip with and without enhanced coseismic weakening, *J. geophys. Res.: Sol. Earth,* **119,** 1986–2004.
Tse, S.T. & Rice, J.R., 1986. Crustal earthquake instability in relation to the depth variation of frictional slip properties, *J. geophys. Res.: Sol. Earth,* **91,** 9452–9472.
Valdez, R. II, Kitajima, H. & Saffer, D., 2019. Effects of temperature on the frictional behavior of material from the Alpine Fault zone, New Zealand, *Tectonophys.,* **762,** 17–27.
Wang, S., 2024. Toward quantitative characterization of simulated earthquake-cycle complexities, *Scientific Rep.,* **14,** 16811.
Ward, S.N., 2012. ALLCAL earthquake simulator, *Seismol. Res. Lett.,* **83,** 964–972.
Warren-Smith, E., Townend, J., Chamberlain, C., Boulton, C. & Michailos, K., 2022. Heterogeneity in microseismicity and stress near rupture-limiting section boundaries along the late-interseismic alpine fault, *J. geophys. Res.: Sol. Earth,* **127,** e2022JB025219.
Wu, Y. & Chen, X., 2014. The scale-dependent slip pattern for a uniform fault model obeying the rate-and state-dependent friction law, *J. geophys. Res.: Sol. Earth,* **119,** 4890–4906.
Yun, J., Gabriel, A.A., May, D.A. & Fialko, Y., 2025. Effects of stress and friction heterogeneity on spatiotemporal complexity of seismic and aseismic slip on strike-slip faults, *J. geophys. Res.: Sol. Earth,* **130,** e2025JB031270.

APPENDIX A:

A1 Model reproducibility and computational implementation

Given how sensitive rate-state cycle models are to details of the discretization (Section 3.1), some numerical quirks can result. While the exact reproduction of a numerical computation will give the same answer for a given hardware, round-off errors may lead to bit wise different results for certain linear algebra packages due to different combinations of summations, for example, if the model domain is partitioned among different numbers of processors. We typically allocate 25 threads using OpenMP for HACApK for a single compute node. Our tests show that for models exhibiting periodic cycles, round-off errors on the order of $\sim 10^{-10}$ to $\sim 10^{-12}$ do not accumulate significantly, and repeated runs produce identical results (Fig. A1). However, for irregular cycles, such small numerical perturbations even due to different numbers of cores, or sequence of summation in parallel, can grow exponentially over longer cycle timescales, as might be expected from a truly chaotic system, leading to divergence in the model trajectory. The overall statistics of the irregular earthquake cycles—such as the recurrence intervals of events with magnitude 6 and above—remain largely unaffected (92 ± 8 yr). Therefore, when modelling irregular regimes in parallel environments, it is important to also recognize this potential limitation and interpret the results with caution alongside other complicating factors.

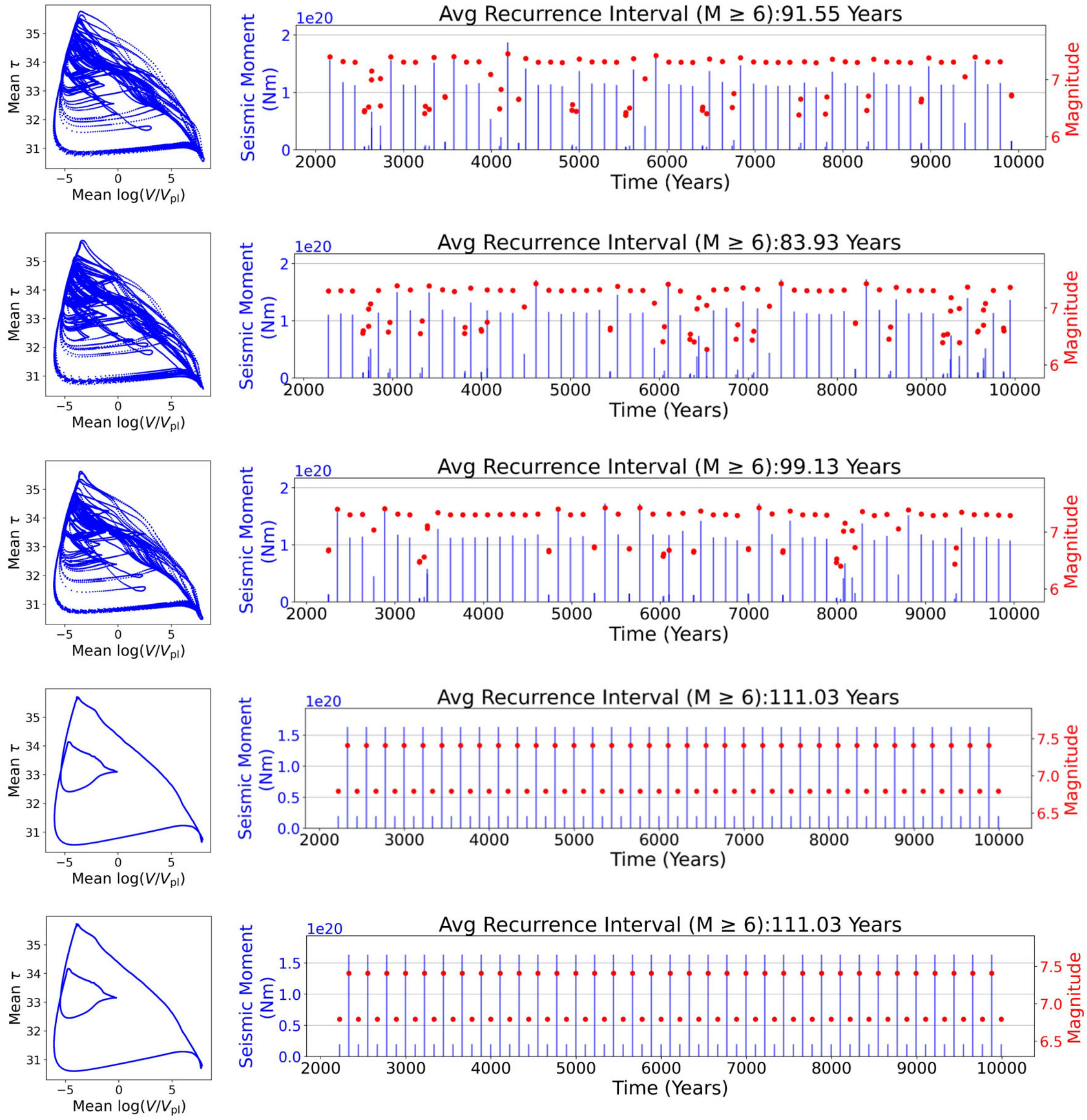

Figure A1. Repeat runs of two models with different frictional setups, executed using HBI and HACApk on OpenMP with 25 threads. The top three rows show three repeat runs of the model that produces an irregular cycle, while the bottom two rows show repeat runs of the model that produces a periodic cycle. Each row displays phase-space trajectories of velocity and shear stress, the seismic moment release time-series, and the magnitudes of individual events. The average recurrence interval of events with $M \geq 6$ is labelled for each run. The irregular-cycle model shows variability among repeats, whereas the periodic-cycle model produces identical results across runs.

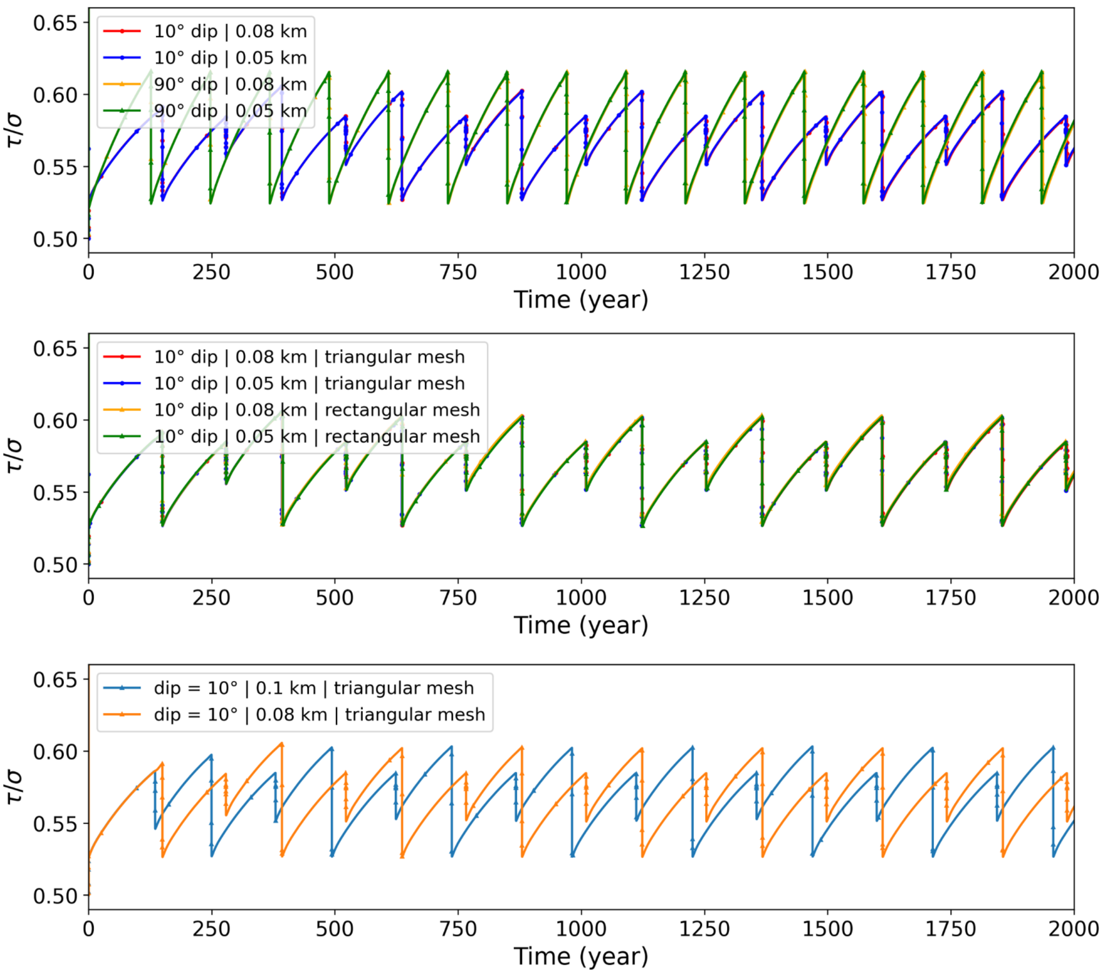

Figure A2. Convergence tests for both rectangular and triangular mesh, as well as both vertical and dipping faults.